Scalar Resonances near 650 and 95 GeV in the GNMSSM with Correct Dark Matter Relic Abundance

Jingwei Lian*1,2, Yao-Bei Liu¹

E-mail: lianjw@hist.edu.cn

Abstract: Recent CMS analyses report an excess in the diphoton-plus- $b\bar{b}$ channel, indicative of a heavy resonance around 650 GeV decaying into a Standard Model (SM)-like Higgs boson and a lighter scalar near 95 GeV. The case for a 95 GeV state is further supported by diphoton excesses observed by both CMS and ATLAS, as well as a $b\bar{b}$ excess previously observed at the Large Electron-Position collider. This study present a unified interpretation of these anomalies within the framework of the General Next-to-Minimal Supersymmetric Standard Model that naturally accommodates a light singlet-dominated CP-even scalar boson near 95 GeV and an heavier doublet-like scalar boson near 650 GeV. Through a comprehensive scan of the parameter space, we demonstrate that the model can explain these excesses at 2σ level while satisfying constraints from the dark matter relic density, direct detection experiments, the properties of the 125 GeV Higgs boson, B-physics observables, and searches for electroweakinos at the Large Hadron Collider (LHC). The interpretation features a Bino-dominated lightest neutralino as the dark matter candidate, whose relic abundance is achieved primarily via A_s funnel annihilation or coannihilation with \tilde{S} -like $\tilde{\chi}_2^0$ s into $h_s A_H$ final states. Our findings provide clear predictions for testing this scenario at the high-luminosity LHC and future colliders.

¹Henan Institute of Science and Technology, Xinxiang 453003, P.R. China

²Department of Physics, Henan Normal University, Xinxiang 453007, P.R. China

^{*}Corresponding author.

\mathbf{C}	ontents	
1	Introduction	1
2	Theoretical preliminaries	3
	2.1 The Superpotential of the GNMSSM	3
	2.2 Higgs Sector	4
	2.3 Neutralino Sector	6
3	Explanation of the excesses	7
	3.1 Strategy in scanning the parameter space	7
	3.2 Numerical Results	10
4	Conclusion	17

1 Introduction

The monumental discovery of the Higgs boson at the Large Hadron Collider (LHC) in 2012 confirmed the existence of a scalar field responsible for electroweak symmetry breaking (EWSB) and mass generation. Although the measured properties of the 125 GeV Higgs boson are broadly consistent with Standard Model (SM) predictions, persistent theoretical issues—most notably the hierarchy problem—continue to motivate the exploration of physics beyond the Standard Model (BSM). Supersymmetry (SUSY) remains a compelling BSM framework, as it provides a natural solution to the hierarchy problem and typically necessitates an extended Higgs sector that predicts the existence of additional scalar states. The search for these new states is paramount, as their observation would provide essential insights into the structure of EWSB and the realization of BSM models.

Intriguingly, several collider experiments have reported persisting hints of such additional scalar states. The first suggestion emerged from LEP experiments, where combined searches for the SM Higgs boson revealed a mild excess in the process $e^+e^- \to Z^* \to Z + b\bar{b}$ for Higgs masses in the range 95-100 GeV. This corresponded to a local significance of 2.3σ and a signal strength [1–3]:

$$\mu_{b\bar{b}}^{\rm exp} = 0.117 \pm 0.057.$$
 (1.1)

This initial hint gained traction with a subsequent observation by CMS at the LHC, which reported an excess in the diphoton ($\gamma\gamma$) channel near 97 GeV during Run 1, carrying a local significance of approximately 2.0 σ [4]. Most recently, the case for this light scalar has been significantly reinforced using the full Run 2 dataset. Both the CMS and ATLAS collaborations, employing advanced analysis techniques, have observed a consistent excess

at an invariant mass of $m_{\gamma\gamma} = 95.4$ GeV [5, 6]. The combined signal strength is now interpreted as a 3.1 σ local excess with a signal rate [7]:

$$\mu_{\gamma\gamma}^{\rm exp} \equiv \mu_{\gamma\gamma}^{\rm ATLAS+CMS} = \frac{\sigma(pp \to \phi \to \gamma\gamma)}{\sigma_{\rm SM}(gg \to H_{\rm SM} \to \gamma\gamma)} = 0.24^{+0.09}_{-0.08}, \tag{1.2}$$

where, ϕ denotes a hypothetically non-SM scalar with mass $m_{\phi} = 95.4$ GeV responsible for the diphoton excess, and $\sigma_{\rm SM}$ refers to the cross section expected for an SM-like Higgs boson $H_{\rm SM}$ of the same mass. Additional phenomenological support for an about 95 GeV state arises from a mild surplus in the di- τ channel observed by CMS [8] and a potential excess in WW final states [9]. Collectively, these observations strengthen the case for the existence of a light scalar resonance around 95 GeV.

Complementing these hints at low mass, a recent search by CMS has unveiled an inter-connected anomaly — a 3.8σ local excess in the search channel featuring a diphoton a diphoton and a $b\bar{b}$ pair. This signal is attributed to the decay of a heavy resonance X near 650 GeV into a SM-like Higgs boson and a BSM scalar ϕ in the 90–100 GeV mass range [10]. The observed production cross section times branching fraction is [11]:

$$\sigma_{\gamma\gamma b\bar{b}} = \sigma(gg \to X \to H_{\rm SM}(\gamma\gamma) + \phi(b\bar{b})) = 0.35^{+0.17}_{-0.13} \text{ fb.}$$
 (1.3)

It is critical to consider constraints from complementary final states. Specifically, a prior CMS search in the $\tau\bar{\tau}$ plus $b\bar{b}$ channel [12] imposes a stringent upper 95% CL limit of approximately 3 fb on the cross section $\sigma(X \to H_{\rm SM}(\tau\bar{\tau}) + \phi(b\bar{b}))$. This translates into an upper 95% CL limit of about 0.1 fb on $\sigma_{\gamma\gamma b\bar{b}}$ [11], suggesting a tension between the observed excess and current limits from related channels.

These collective anomalies have sparked extensive investigations across various BSM scenarios [3, 7, 11, 13–68]. In particular, several works [11, 18, 31, 68] have explored the possible connection between the 95 GeV and 650 GeV excesses. Among the proposed explanations, the Next-to-Minimal Supersymmetric Standard Model (NMSSM) [69, 70] stands out as a particularly attractive and economical framework for accommodating these scalar states and furnishing proper Dark Matter (DM) candidates. Previous NMSSM studies with a \mathbb{Z}_3 symmetry have investigated both mass excesses [11, 71], though typically under the assumption that the observed DM relic density receives additional contributions beyond the lightest supersymmetric particle (LSP). The general form of the NMSSM, termed as "GNMSSM", includes \mathbb{Z}_3 -violating terms that naturally address the tadpole and domain-wall problems [69]. The enlarged parameter space, featuring ten parameters in the Higgs sector, offers the necessary flexibility to account for both the 95 GeV and 650 GeV excesses, while also providing a rich phenomenology for the Singlino/Bino Dark Matter sector. The \mathbb{Z}_3 -breaking terms also modify the Higgsino and Singlino masses, significantly influencing the DM sector. Our recent work [55, 59] has shown that the 95 GeV excesses can be consistently explained in the GNMSSM through a Singlino-dominated LSP that saturates the observed DM relic density without violating existing experimental constraints.

The goal of this paper is to determine to what extent the 95 GeV and 650 GeV excesses can be simultaneously explained within the GNMSSM while remaining compatible with current LHC data and the recent null results from the LZ dark-matter experiment. In

this framework, the heavy CP-even Higgs boson with mass near 650 GeV decays into a SM-like Higgs boson and a light singlet-dominated CP-even Higgs boson with mass around 95 GeV. We demonstrate that the GNMSSM can simultaneously account for the LEP, CMS, and ATLAS hints of a 95 GeV scalar as well as the CMS diphoton plus $b\bar{b}$ excess near 650 GeV at the 2σ level. We further identify parameter regions in which a Binodominated neutralino constitutes a viable thermal DM candidate, potentially testable by the forthcoming sensitivity of direct-detection experiments.

The remainder of this paper is organized as follows. In Sec. 2, we briefly recapitulate the basics of the GNMSSM framework and the predicted signal rates for the anomalies. In Sec. 3, we perform a sophisticated scan over the model parameter space and present detailed numerical results. Finally, our conclusions are summarized in Sec. 4.

2 Theoretical preliminaries

2.1 The Superpotential of the GNMSSM

The NMSSM is known as a straightforward and well-motivated extension of the Minimal Supersymmetric Standard Model (MSSM), achieved by introducing a gauge-singlet chiral superfield. Its appeal stems not only from providing a natural solution to the so-called μ -problem inherent in the MSSM, but also from offering an expanded and often more viable DM sector [72–74]. Crucially, the NMSSM contributes to a sizeable mass lift for the SM-like Higgs boson. Especially in scenarios involving a light CP-even Higgs, this mass can be elevated by both an additional tree-level contribution and a large singlet-doublet mixing [75–77], mitigating the need for substantial radiative corrections from top/stop loops. The GNMSSM incorporates the most general renormalizable couplings in its superpotential [69]

$$W_{\text{GNMSSM}} = W_{\text{Yukawa}} + \lambda \hat{S} \hat{H}_u \cdot \hat{H}_d + \frac{\kappa}{3} \hat{S}^3 + \mu \hat{H}_u \cdot \hat{H}_d + \frac{1}{2} \mu' \hat{S}^2 + \xi \hat{S}, \tag{2.1}$$

where W_{Yukawa} contains the quark and lepton Yukawa terms in the MSSM superpotential, $\hat{H}_u = (\hat{H}_u^+, \hat{H}_u^0)^T$ and $\hat{H}_d = (\hat{H}_d^0, \hat{H}_d^-)^T$ are the $SU(2)_L$ Higgs doublet superfields, and \hat{S} is the singlet superfield. The dimensionless parameters λ and κ play roles analogous to those in the \mathbb{Z}_3 -invariant NMSSM, while the bilinear mass terms μ and μ' and the singlet tadpole term ξ explicitly break the \mathbb{Z}_3 symmetry. These \mathbb{Z}_3 -breaking terms are advantageous, as they are essential for resolving the tadpole problem [69, 78] and the cosmological domainwall problem that plagues the \mathbb{Z}_3 -NMSSM [79–81]. Since one among μ , μ' , and ξ may be eliminated through a shift of the \hat{S} field followed by a redefinition of the remaining parameters [82], we set $\xi = 0$ without loss of generality. The bilinear parameters μ and μ' may naturally reside at the electroweak scale, originating from an underlying discrete R-symmetry Z_4^R after supersymmetry breaking [82–85].

2.2 Higgs Sector

The soft SUSY-breaking Lagrangian for the Higgs fields in the GNMSSM takes the form:

$$-\mathcal{L}_{soft} = \left[\lambda A_{\lambda} S H_u \cdot H_d + \frac{1}{3} \kappa A_{\kappa} S^3 + m_3^2 H_u \cdot H_d + \frac{1}{2} m_S'^2 S^2 + \xi' S + h.c. \right] + m_{H_u}^2 |H_u|^2 + m_{H_d}^2 |H_d|^2 + m_S^2 |S|^2,$$
(2.2)

Here, H_u , H_d , and S denote the scalar components of the Higgs superfields, and $m_{H_u}^2$, $m_{H_d}^2$, and m_S^2 are their soft-breaking masses. After solving the EWSB conditional equations to minimize the scalar potential and expressing these soft masses in terms of the vacuum expectation values (vevs), namely, $\langle H_u^0 \rangle = v_u/\sqrt{2}$, $\langle H_d^0 \rangle = v_d/\sqrt{2}$, and $\langle S \rangle = v_s/\sqrt{2}$, with $v = \sqrt{v_u^2 + v_d^2} \simeq 246$ GeV and $\tan \beta \equiv v_u/v_d$, the Higgs sector is governed by eleven independent parameters: $\tan \beta$, v_s , the Yukawa couplings λ and κ , the soft-breaking trilinear coefficients A_{λ} and A_{κ} , the bilinear mass parameters μ and μ' , the soft-breaking parameters m_3^2 and $m_S'^2$, and the soft-breaking tadpole coefficient ξ' that is assumed to vanish the present analysis.

To clearly delineate the properties of the Higgs states, it is convenient to use rotated field combinations: $H_{\rm SM} \equiv \sqrt{2} {\rm Re} (\sin \beta H_u^0 + \cos \beta H_d^0)$, $H_{\rm NSM} \equiv \sqrt{2} {\rm Re} (\cos \beta H_u^0 - \sin \beta H_d^0)$, and $A_{\rm NSM} \equiv \sqrt{2} {\rm Im} (\cos \beta H_u^0 - \sin \beta H_d^0)$, where $H_{\rm SM}$ behaves like the SM Higgs field, and $H_{\rm NSM}$ and $A_{\rm NSM}$ describing the additional doublet fields [77]. The singlet field remains unrotated and is written as $\sqrt{2}S \equiv H_{\rm S} + iA_S$.

In the basis $(H_{NSM}, H_{SM}, Re[S])$, the elements of the symmetric squared mass matrix for the CP-even Higgs boson can be written in the following forms [69, 86]:

$$\mathcal{M}_{S,11}^{2} = m_{A}^{2} + \frac{1}{2}(2m_{Z}^{2} - \lambda^{2}v^{2})\sin^{2}2\beta,$$

$$\mathcal{M}_{S,12}^{2} = -\frac{1}{4}(2m_{Z}^{2} - \lambda^{2}v^{2})\sin 4\beta,$$

$$\mathcal{M}_{S,13}^{2} = \sqrt{2}\lambda\mu_{tot}v(\delta - 1)\cot 2\beta,$$

$$\mathcal{M}_{S,22}^{2} = m_{Z}^{2}\cos^{2}2\beta + \frac{1}{2}\lambda^{2}v^{2}\sin^{2}2\beta,$$

$$\mathcal{M}_{S,23}^{2} = \sqrt{2}\lambda\mu_{tot}v\delta,$$

$$\mathcal{M}_{S,33}^{2} = m_{B}^{2},$$
(2.3)

while those for the CP-odd Higgs boson in the basis (A_{NSM}, A_S) are:

$$\mathcal{M}_{P,11}^2 = m_A^2, \quad \mathcal{M}_{P,22}^2 = m_C^2, \quad \mathcal{M}_{P,12}^2 = \frac{\lambda v}{\sqrt{2}} (A_\lambda - m_N).$$
 (2.4)

We inroduc a δ factor in $\mathcal{M}_{S,13}^2$ and $\mathcal{M}_{S,23}^2$, defined as:

$$\delta \equiv 1 - \frac{(A_{\lambda} + m_N)\sin 2\beta}{2\mu_{tot}},\tag{2.5}$$

with the Higgsino mass $\mu_{tot} \equiv \mu_{eff} + \mu = \lambda v_s / \sqrt{2} + \mu$ and the Singlino mass $m_N \equiv \sqrt{2\kappa v_s} + \mu'$, to simplify the expression and allow for direct manipulation of the mixings

of $H_{\rm S}$ with $H_{\rm SM}$ and $H_{\rm NSM}$. This factor is expected to be tiny in the alignment without decoupling limit [53, 87]. m_A is the typical definition of the mass of the doublet-like pseudoscalar Higgs field. m_B and m_C characterize the singlet-like CP-even, and the singlet-like CP-odd Higgs masses, respectively. Then the soft-breaking parameters A_{κ} , m_3^2 and $m_S'^2$ can be expressed in terms of the physical input parameters:

$$A_{\kappa} = \frac{2m_{B}^{2}}{m_{N} - \mu'} + \frac{\lambda^{2}v^{2}}{4\kappa\mu_{eff}^{2}} \left[(A_{\lambda} + \mu')\sin 2\beta - 2\mu \right] - 2m_{N} - \mu',$$

$$m_{3}^{2} = \frac{1}{2} \left[m_{A}^{2}\sin 2\beta - \mu_{eff}(2A_{\lambda} + m_{N} + \mu') \right],$$

$$m_{S}^{\prime 2} = \frac{1}{2} \left[m_{B}^{2} - m_{C}^{2} + \lambda\kappa v^{2}\sin 2\beta - (m_{N} - \mu')(2A_{\kappa} + m_{N} + \mu') \right]. \tag{2.6}$$

Note that the mass parameter for the singlet-like CP-odd Higgs m_C is fixed at 800GeV in this study for simplicity to be consistent with current collider experimental limitations [8, 88].

Diagonalizing the squared mass matrix with mixing angles, denoted as $V_{h_i}^j$, yields three CP-even Higgs mass eigenstates:

$$h_i = V_{h_i}^{\text{NSM}} H_{\text{NSM}} + V_{h_i}^{\text{SM}} H_{\text{SM}} + V_{h_i}^{\text{S}} H_{\text{S}},$$
 (2.7)

with $h_i = \{h_{\rm s}, h, H\}$ ordered by ascending mass. The second CP-even mass eigenstate h corresponds to the observed 125 GeV SM-like Higgs boson. This state is predominantly composed of the $H_{\rm SM}$ component, requiring contributions from $H_{\rm NSM}$ and ${\rm Re}[S]$ components restricted to be less than about 10% [89, 90], i.e., $\sqrt{\left(V_h^{\rm NSM}\right)^2 + \left(V_h^{\rm S}\right)^2} \lesssim 0.1$ and $|V_h^{\rm SM}| \sim 1$ consistent with current Higgs data. In addition, the imaginary components A_S and $A_{\rm NSM}$ mix into two CP-odd Higgs mass eigenstates $a_i = \{A_H, A_s\}$, while the charged components give rise to a pair of charged Higgs bosons H^\pm . The light CP-odd Higgs boson A_H and the charged Higgs bosons H^\pm should exhibit a nearly degenerate mass with the heavy CP-even boson H.

The present study assumes that the lightest CP-even Higgs boson h_s is singlet-dominated and fully accounts for both the $\gamma\gamma$ and $b\bar{b}$ excesses near 95.4 GeV. The signal strengths normalized to their SM predictions are [55]:

$$\mu_{\gamma\gamma}|_{m_{h_s}=95.4 \text{ GeV}} = \frac{\sigma_{\text{SUSY}}(pp \to h_s)}{\sigma_{\text{SM}}(pp \to h_s)} \times \frac{\text{Br}_{\text{SUSY}}(h_s \to \gamma\gamma)}{\text{Br}_{\text{SM}}(h_s \to \gamma\gamma)},$$
 (2.8)

$$\mu_{b\bar{b}}|_{m_{h_s}=95.4 \text{ GeV}} = \frac{\sigma_{\text{SUSY}}(e^+e^- \to Zh_s)}{\sigma_{\text{SM}}(e^+e^- \to Zh_s)} \times \frac{\text{Br}_{\text{SUSY}}(h_s \to b\bar{b})}{\text{Br}_{\text{SM}}(h_s \to b\bar{b})}, \tag{2.9}$$

where the mass of h_s is fixed at 95.4 GeV. The production rate $\sigma(pp \to h_s)$ and the decay branching ratio $\text{Br}(h_s \to \gamma \gamma)$ labeled with the subscript 'SUSY' refer to the predictions from the model, whereas those with the subscript 'SM' assume SM couplings for h_s .

The $\gamma\gamma b\bar{b}$ excess near 650 GeV can be attributed to the heavy doublet-dominated CP-even Higgs boson H decaying into a SM-like Higgs boson h and a singlet-dominated Higgs boson h_s . The cross section of the resonance in the $\gamma\gamma b\bar{b}$ channel can be expressed

as follows:

$$\sigma_{\gamma\gamma b\bar{b}} = \sigma(gg \to H) \times \text{Br}_{\text{SUSY}}(H \to hh_s) \times \text{Br}_{\text{SUSY}}(h \to \gamma\gamma) \times \text{Br}_{\text{SUSY}}(h_s \to b\bar{b}), \quad (2.10)$$

where the masses of H, h ad h_s are fixed at approximately 650 GeV, 125 GeV and 95.4 GeV, respectively. By fitting the GNMSSM predictions for $\mu_{\gamma\gamma}$, $\mu_{b\bar{b}}$, and $\sigma_{\gamma\gamma b\bar{b}}$ to the observed experimental rates, we can investigate the viability of the GNMSSM as a unified interpretation for the 95 GeV and 650 GeV excesses.

2.3 Neutralino Sector

The neutralino sector within the GNMSSM framework is comprised of five superpartners: the gaugino fields $(\tilde{B}, \text{ the Bino}, \text{ and } \tilde{W}, \text{ the Wino})$, the Higgsino fields $(\tilde{H}_d^0 \text{ and } \tilde{H}_u^0)$, and the Singlino field (\tilde{S}) . In the basis $\psi^T \equiv (\tilde{B}, \tilde{W}, \tilde{H}_d^0, \tilde{H}_u^0, \tilde{S})$, the symmetric 5×5 neutralino mass matrix, \mathcal{M} , is given by [69]:

$$\mathcal{M} = \begin{pmatrix} M_1 & 0 & -m_Z \sin \theta_W \cos \beta & m_Z \sin \theta_W \sin \beta & 0 \\ M_2 & m_Z \cos \theta_W \cos \beta & -m_Z \cos \theta_W \sin \beta & 0 \\ 0 & -\mu_{tot} & -\frac{1}{\sqrt{2}} \lambda v \sin \beta \\ 0 & -\frac{1}{\sqrt{2}} \lambda v \cos \beta \end{pmatrix}, \tag{2.11}$$

where θ_W is the weak mixing angle, and M_1 and M_2 are the soft-breaking masses of the Bino and Wino, respectively. Diagonalizing \mathcal{M} by a rotation matrix N yields five neutralino mass eigenstates:

$$\tilde{\chi}_i^0 = \sum_{j=1}^5 N_{ij} \,\psi_j^0, \qquad i = 1, \dots, 5,$$
(2.12)

ordered by increasing mass. The element N_{ij} parametrizes the contribution of the interaction eigenstate ψ_j^0 to the physical neutralino $\tilde{\chi}_i^0$. Under R parity conservation, the lightest neutralino $\tilde{\chi}_1^0$ is stable and constitutes a viable dark matter (DM) candidate when it is the Lightest Supersymmetric Particle (LSP). In many NMSSM realizations, a Singlino-dominated LSP naturally reproduces the observed relic abundance while evading stringent direct detection bounds [91]. In the present study, however, this possibility is strongly limited. The relatively large value of λ required to account for both the excesses enhances the Higgs-mediated scattering cross section of a Singlino-like LSP, bringing it into tension with current direct detection limits [74, 92]. Furthermore, the mixing constraints on $V_{h_i}^{\rm SM}$ and $V_{h_i}^{\rm NSM}$ required by the 95 GeV and 650 GeV anomalies further reduce the viable parameter space for Singlino-like DM. In contrast, as will be demonstrated later, the combined interpretation of the excesses instead favors a Bino-dominated LSP. Such a Bino-like neutralino can efficiently reduce its relic abundance through Higgs-funnel annihilation and/or coannihilations with Singlino-, Higgsino-, or Wino-like electroweakinos, while remaining consistent with direct detection constraints.

3 Explanation of the excesses

This section outlines the parameter-sampling strategy and presents detailed numerical results that account for the observed excesses in the diphoton and $b\bar{b}$ final states—both separately and simultaneously—while remaining consistent with other experimental constraints, in particular those from Higgs data and dark matter detections. The numerical procedure follows several steps. First, we implement the GNMSSM using SARAH-4.14.3 [93–96] to generate analytical model files. Second, the packages SPheno-4.0.5 [97, 98] and FlavorKit [99] are used to compute the SUSY mass spectrum and low-energy flavor observables, respectively. Subsequently, dark matter observables—including relic density, annihilation channels, and direct detection rates—are evaluated with MicrOMEGAs-5.0.4 [100–109]. Finally, the resulting samples are then analyzed using both Bayesian and Frequentist statistical frameworks: the posterior probability density function (PDF) and the profile likelihood (PL) [110]. These complementary approaches provide a robust characterization of the viable parameter space and enable a nuanced interpretation of the experimental anomalies.

3.1 Strategy in scanning the parameter space

To thoroughly investigate the phenomenological implications of the observed excesses and DM constraints, we employ a sophisticated scan strategy focusing on phenomenologically relevant input parameters. The scan includes all parameters relevant to the Higgs sector. However, instead of directly scanning the original soft-breaking parameters $(m_3^2, A_{\kappa}, A_{\lambda})$ appearing in Eq. (2.2), we trade them for the physical and semi-physical masses and mixing terms $(m_A, m_B, \text{ and } \delta)$ as defined in Eqs. (2.6) and (2.5). This substitution improves the efficiency of the sampling by allowing direct exploration of regions consistent with a target Higgs mass spectrum while preserving the essential physics. The soft trilinear couplings of the third-generation squarks, A_t and A_b , are treated as free parameters because of their crucial impact on the radiative corrections to the SM-like Higgs mass. Furthermore, the soft gaugino masses M_1 and M_2 are included as scan parameters to allow for a Bino-dominated $\tilde{\chi}_1^0$ dark matter candidate, as suggested by the analysis in Sec. 2. In total, the scan explores a 12-dimensional parameter space as delineated in Table 1. The parameter ranges are carefully determined based on theoretical considerations and exploratory trial scans across broader intervals to ensure both comprehensive coverage and effective exploration of the regions of interest. All final samples are required to respect the constraint of field-theoretic perturbativity between the electroweak and GUT scales. The approximate bound derived for the \mathbb{Z}_3 -NMSSM [86], $\lambda^2 + \kappa^2 \lesssim 0.5$, is applied here, as the GNMSSM beta functions do not introduce new scale-dependent contributions up to the two-loop level (see Appendices in Refs. [69, 111, 112]). All numerical results presented in this work are ensured to satisfy this condition.

The multi-dimensional parameter space is explored using the MultiNest algorithm [113, 114], a highly efficient nested sampling method, with a fixed number of live points set to nlive = 6000 to ensure comprehensive survey and accurate computation of the Bayesian evidence and posterior distributions¹. The likelihood function guiding the scan is

¹In nested sampling algorithms, *nlive* denotes the number of active (live) points used to define successive

Table 1. Ranges of input parameters used in this study. All parameters are assigned flat priors due to their well-defined physical interpretation. The soft trilinear coefficients for third-generation squarks are unified as $A_t = A_b$. Dimensional parameters not directly relevant here are fixed to simplify the analysis and comply with experimental constraints: the gluino mass is set to $M_3 = 3$ TeV, and other unspecified parameters are fixed at 2 TeV to satisfy LHC limits on SUSY particles. All parameters are defined at the renormalization scale $Q_{\rm input} = 1$ TeV.

Parameter	Prior	Range	Parameter	Prior	Range
λ	Flat	$0.5 \sim 0.7$	$\mu_{tot}/{\rm GeV}$	Flat	$500.0 \sim 1000$
κ	Flat	$-0.5 \sim 0.5$	$\mu_{eff}/{\rm GeV}$	Flat	$-1000 \sim 1000$
δ	Flat	$-0.05 \sim 0.05$	$m_A/{ m GeV}$	Flat	$500.0 \sim 650.0$
$\tan \beta$	Flat	$1.0 \sim 2.0$	$m_B/{ m GeV}$	Flat	$90.0 \sim 120$
$M_1/{ m GeV}$	Flat	$-1000 \sim -200.0$	$A_t/{ m GeV}$	Flat	$1000 \sim 3000$
$M_2/{ m GeV}$	Flat	$200.0 \sim 1000$	$m_N/{ m TeV}$	Flat	$-1000 \sim 1000$

constructed as $\mathcal{L} \equiv \mathcal{L}_{650+95} \times \mathcal{L}_{Res}$. The first factor $\mathcal{L}_{650+95} = \exp(-\frac{1}{2}\chi_{650+95}^2)$ quantifies the compatibility of the GNMSSM predictions with the central values and uncertainties of the experimental observations of the $\gamma\gamma$ plus $b\bar{b}$ excesses near 650GeV and the 95GeV diphoton and $b\bar{b}$ excesses, via a χ^2 function:

$$\chi_{650+95}^2 = \left(\frac{\sigma_{\gamma\gamma b\bar{b}} - 0.35}{0.13}\right)^2 + \left(\frac{\mu_{\gamma\gamma} - 0.24}{0.08}\right)^2 + \left(\frac{\mu_{b\bar{b}} - 0.117}{0.057}\right)^2. \tag{3.1}$$

The second factor, \mathcal{L}_{Res} term enforces essential physical and experimental bounds by acting as a step function: $\mathcal{L}_{Res} = 1$ if all conditions are met, and $\mathcal{L}_{Res} = \exp[-100]$ otherwise. The required restrictions include:

- Masses of the three scalars: To interprete the observed excesses, we impose specific mass requirements on the three CP-even Higgs bosons:
 - Light Scalar (h_s): The mass of the light, singlet-like scalar is required to be in the range 95.4 ± 1 GeV to align with the experimental hints.
 - Heavy Resonance (H): The heavy scalar mass is constrained to the range 650 ± 25 GeV to match the resonant excess observed by CMS [10, 11].
 - SM-like Higgs (h): The mass of the SM-like Higgs boson must be consistent with the LHC measurements, allowing for a ± 3 GeV tolerance to account for combined experimental and theoretical uncertainties.
- SM-like Higgs data fit: The SM-like Higgs boson must satisfy the ATLAS and CMS measurements at the 95% confidence level. This condition is validated using the newest version of the HiggsTools code that incorporates the HiggsSignals-2 [115–118], which compares model predictions to a full set of current measurements of the 125GeV Higgs properties and returns a χ^2 value that quantifies the agreement of the model predictions with the measurements. Samples satisfying the condition $\Delta\chi^2_{125} \equiv$

iso-likelihood contours [113, 114]. Larger values of *nlive* improve the resolution of the parameter space at the cost of increased computational time.

 $\chi^2 - \chi^2_{125, \rm SM} \lesssim 6.18$ where $\chi^2_{125, \rm SM} = 153$ is the SM fit result, would be considered valid as they provide a good description of the Higgs data at an approximate 2σ C.L. (assuming Gaussian uncertainties) [119].

- Extra Higgs searches: Signal rates for all non-SM Higgs bosons (h_s, H, A_H, H^{\pm}) must comply with cross-section limits based on experimental data at LEP, Tevatron, and the LHC. This requirement is implemented using the HiggsTools code [120] with the complete HiggsBounds-5.10.2 library [121–125].
- **DM relic density:** The predicted DM relic density must agree with the with the Planck-2018 central value ($\Omega h^2 = 0.120$) [126], allowing for a conservative 20% theoretical uncertainty: $0.096 \le \Omega h^2 \le 0.144$.
- **DM detections:** The spin-independent (SI) and spin-dependent (SD) $\tilde{\chi}_1^0$ -nucleon scattering cross-sections must be below the currently most stringent upper bounds imposed by the LZ experiments [127, 128]. Constraints from DM indirect searches are not considered here as they are less restrictive for the masses under consideration ($|m_{\tilde{\chi}_1^0}| \gtrsim 100 \text{ GeV}$) [129].
- B-physics observables: The branching ratios $B_s \to \mu^+\mu^-$ and $B \to X_s\gamma$ are required to agree with current experimental measurements at the 2σ level [130].
- Vacuum stability: The electroweak vacuum must be demonstrated to be either the global minimum or a sufficiently long-lived, metastable vacuum state [131]. This is rigorously tested using the VevaciousPlusPlus code [132, 133].

Constraints from LHC searches for electroweakinos are expected to have a negligible impact on the scan results. This is because the gaugino–Higgsino states in Table 1 lie in relatively heavy mass ranges, and all other SUSY particles are assumed to be heavy and decoupled. This estimation is consistent with recent statistical combinations of ATLAS Run 2 searches [134]. To confirm this, we evaluate all sampled points using SModelS-3.0.0, which implements a wide set of simplified-model constraints by decomposing SUSY signatures into experimentally tested topologies and applying the corresponding efficiency maps [135]. Furthermore, four representative benchmark points are subjected to dedicated Monte Carlo simulations. For each benchmark, 10⁶ events were generated with MadGraph_aMC@NLO [136, 137] for the following electroweakino production channels:

$$pp \to \tilde{\chi}_{i}^{0} \tilde{\chi}_{j}^{\pm}, \quad i = 2, 3, 4, 5; \quad j = 1, 2$$

$$pp \to \tilde{\chi}_{i}^{\pm} \tilde{\chi}_{j}^{\mp}, \quad i, j = 1, 2;$$

$$pp \to \tilde{\chi}_{i}^{0} \tilde{\chi}_{j}^{0}, \quad i, j = 2, 3, 4, 5.$$
(3.2)

Production cross sections are computed at next-to-leading order using Prospino2 [138]. Parton showering and hadronization are performed with PYTHIA8 [139], and detector effects are simulated using Delphes [140]. The resulting events are analyzed with CheckMATE-2.0.26 [141–143], which computes the R value, defined as the exclusion ratio $R \equiv max\{S_i/S_{i.obs}^{95}\}$, with

 S_i representing the simulated event number of the *i*-th signal region (SR), and $S_{i,obs}^{95}$ the corresponding 95% confidence level upper limit. Values of R > 1 indicates exclusion (neglecting theoretical and experimental uncertainties) [144], while R < 1 denotes consistency with current experimental analyses. The specific ATLAS and CMS analyses used in this study are listed in Table A1 in the Appendix.

3.2 Numerical Results

The scan process yields ver 25,000 parameter samples that satisfy all applied theoretical and experimental constraints. A key result across all viable samples is the preference for the Bino-dominated $\tilde{\chi}^0_1$ as the Dark Matter (DM) candidate. These samples naturally cluster into two distinct scenarios according to the dominant mechanism responsible for achieving the observed relic abundance.:

- Scenario I ($\approx 92\%$): Achieves the correct relic density primarily via A_s funnel annihilation or coannihilation with \tilde{S} -like $\tilde{\chi}_2^0$ s, typically into the $h_s A_H$ final state.
- Scenario II ($\approx 8\%$): Achieves the correct relic density through coannihilation with \tilde{H} -like $\tilde{\chi}_2^0$ s or $\tilde{\chi}_1^{\pm}$ s, favoring the $h_s A_s$ final state.

The correlation between the cross section $\sigma(gg \to H \to hh_s \to \gamma\gamma b\bar{b})$ and the signal strengths $\mu_{\gamma\gamma}$ and $\mu_{b\bar{b}}$ are depicted in the left and right panels in Fig.1, respectively. The orange dashed lines and shaded bands mark the central value of the cross section $\sigma_{\gamma\gamma b\bar{b}}$ with the corresponding 2.0σ uncertainty, and the blue ones mark that of the signal strengths $\mu_{\gamma\gamma}$ and $\mu_{b\bar{b}}$. The purple dashed-dotted contour delineate the combined 2.0σ region on each plane. The plot shows that **Scenario I** can interpret the $\sigma_{\gamma\gamma b\bar{b}}$ excess near 650 GeV and μ_{rr} and $\mu_{b\bar{b}}$ excesses near 95 GeV at the 2σ level at the same time. While samples in **Scenario I** can push the cross section $\sigma(gg \to H \to hh_s \to \gamma\gamma bb)$ value closer to the 1σ range from below, this comes at the cost of shifting μ_{rr} away from the 2σ range. Moreover, these points tend to be excluded by the CMS upper 95% CL limit of approximately 0.1 fb from the $\tau\bar{\tau}$ plus $b\bar{b}$ search [11, 12]. In contrast, $\sigma(gg \to H \to hh_s \to \gamma\gamma b\bar{b})$ in **Scenario** II can reach at most 0.8 fb. Nevertheless, it achieves an overall 2σ fit when combining the $\sigma_{\gamma\gamma b\bar{b}}$ and μ_{rr} excess, i.e., $\chi^2_{\sigma_{\gamma\gamma b\bar{b}}} + \chi^2_{\mu_{rr}} \leq 6.18$. In this scenario, μ_{rr} can reach its central value, whereas $\mu_{b\bar{b}}$ remains below 0.02, though still within the 2σ region. This behavior arises because a suppression of $Br_{SUSY}(h_s \to b\bar{b})$ is needed to enhance the branching ratio $Br_{SUSY}(h_s \to \gamma \gamma)$ and thus a larger μ_{rr} . This also explains the trend seen in the left panel in Fig.1, where $\sigma(gg \to H \to hh_s \to \gamma\gamma bb)$ decreases with μ_{rr} increases. Samples excluded by constraints from the Higgs experiments, DM relic density and direct detections are denoted by grey dots. In particular, the searches for additional Higgs states implemented in HiggsBounds set the strongest limits for $\sigma(gg \to H \to hh_s \to \gamma\gamma b\bar{b}) \gtrsim 0.09$ fb, while the SM-like Higgs precision data encoded in HiggsSignals dominate the exclusions below this threshold. Furthermore, roughly half of the remaining samples are removed by DM relic density and direct detection constraints.

The right panel of in Fig.1 displays a nontrivial correlation between $\sigma(gg \to H \to hh_s \to \gamma\gamma b\bar{b})$ and $\mu_{b\bar{b}}$. This complexity arises because an increase $\text{Br}_{\text{SUSY}}(h_s \to b\bar{b})$ does

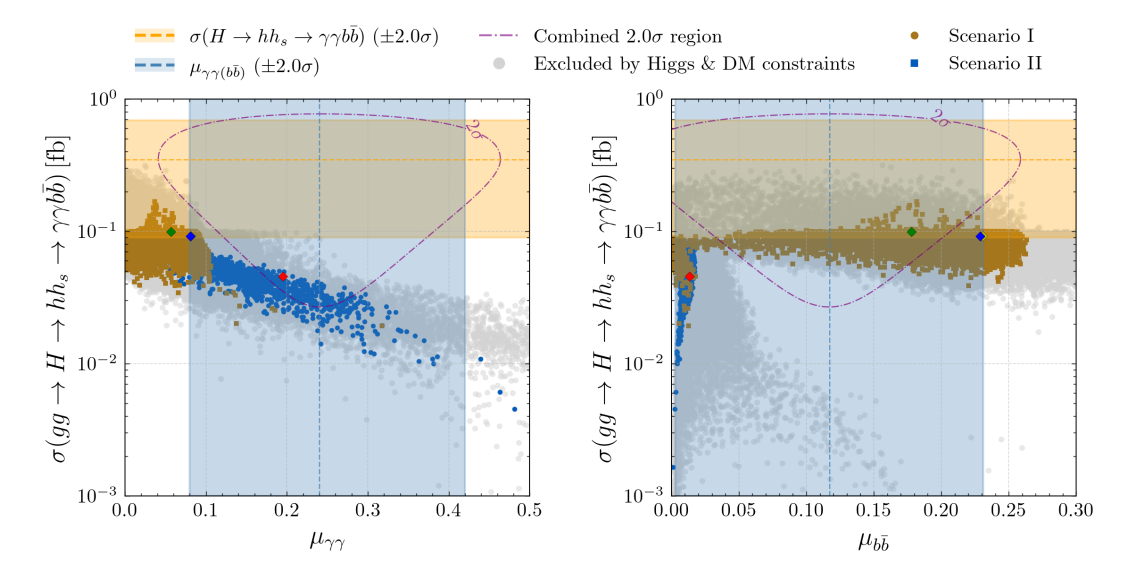


Figure 1. Scattering plots of samples satisfying all applied constraints, projected onto the planes of the cross section $\sigma(gg \to H \to hh_s \to \gamma\gamma b\bar{b})$ versus the signal strengths $\mu_{\gamma\gamma}$ (left) and $\mu_{b\bar{b}}$ (right). The orange dashed lines and shaded bands indicate the central value of $\sigma(gg \to H \to hh_s \to \gamma\gamma b\bar{b})$ in Eq. (1.3) with the corresponding 2σ uncertainty, while the blue lines show the central values of $\mu_{\gamma\gamma}$ in Eq. (1.2) (left) and $\mu_{b\bar{b}}$ in Eq. (1.1) (right). The purple dash-dotted contours mark the combined 2σ regions on each plane. Grey dots represent samples excluded by HiggsSignals, HiggsBounds, or by DM relic density and direct detection constraints. Amber squares and blue dots denote Scenario I and Scenario II, respectively. Colored diamonds correspond to the four benchmark points, with details listed in Table 2 and Table 3. 3.

not necessarily translate into a corresponding enhancement of $\mu_{b\bar{b}}$. In particular, increasing the coupling of h_s to bottom quark pairs $|C_{h_sb\bar{b}}|$ may simultaneously suppress its couplings to the electroweak gauge bosons $|C_{h_sVV}|^2$. Because $\mu_{b\bar{b}}$ depends not only on BrSUSY $(h_s \to b\bar{b})$ but also on the associated suppression of the h_s -Z coupling, $\mu b\bar{b}$ may saturate or even decrease as BrSUSY $(h_s \to b\bar{b})$ grows. Although in most of the parameter space $|C_{h_sb\bar{b}}|$ and $|C_{h_sVV}|$ increase together, the associated reduction of the SM-like Higgs coupling to photons suppresses BrSUSY $(h \to \gamma \gamma)$. This effect offsets the enhancement of $\sigma(gg \to H \to hh_s \to \gamma \gamma b\bar{b})$ expected from increasing BrSUSY $(h_s \to b\bar{b})$, thereby further contributing to the intricate structure in the $\mu_{b\bar{b}}$ - $\sigma(gg \to H \to hh_s \to \gamma \gamma b\bar{b})$ correlation.

Next, we apply the Bayesian inference method to analyze the model predictions for the heavy Higgs boson H near 650 GeV. By accumulating the posterior PDF of samples obtained from the scan process 3 , we find that **Scenario I** and **Scenario II** contribute

$$C_{h_ib\bar{b}} = V_{h_i}^{\rm SM} - V_{h_i}^{\rm NSM} \tan\beta, \quad C_{h_iVV} = V_{h_i}^{\rm SM}, \label{eq:chibb}$$

 C_{h_sVV} may decrease with $C_{h_sb\bar{b}}$ increases when $V_{h_s}^{\rm SM}$ and $V_{h_s}^{\rm NSM}$ share the same sign. In this study, we verify that this behaviour occurs for $0.0 \lesssim C_{h_sb\bar{b}} \lesssim 0.3$. Furthermore, the effective coupling of the SM-like Higgs h to $\gamma\gamma$ decreases from about 1.0 to 0.89 once $C_{h_sb\bar{b}} \gtrsim 0.3$.

²Recalling the normalized couplings of h_i to $b\bar{b}$ and vector bosons V = W, Z at tree level in terms of the mixing coefficients $V_{h_i}^j$ in Eq.(2.7):

³The nested sampling algorithm used in this work transforms the multidimensional evidence integral

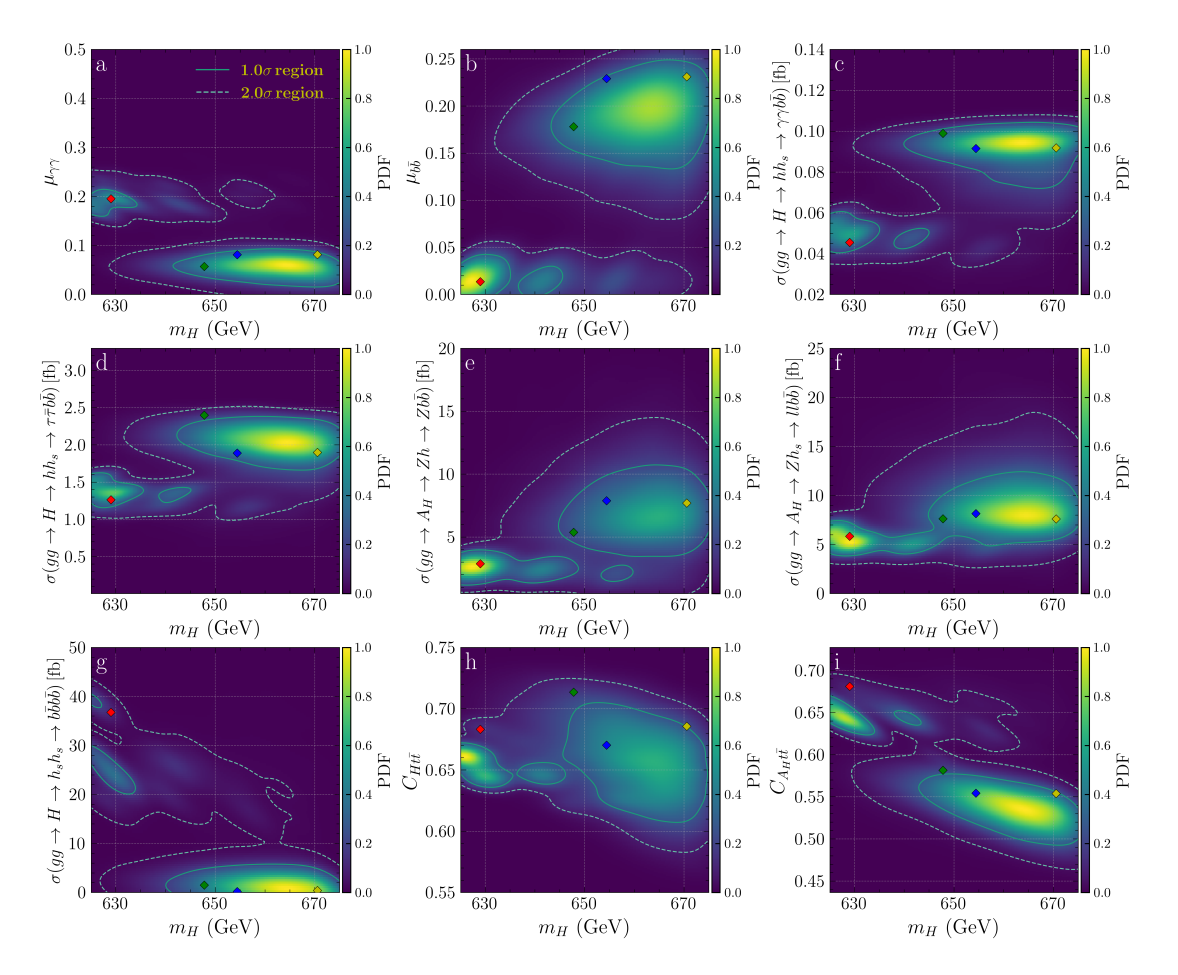


Figure 2. Two-dimensional posterior PDF distributions of the heavy Higgs boson mass m_H versus (a) $\mu_{\gamma\gamma}$, (b) $\mu_{b\bar{b}}$, (c) $\sigma(gg \to H \to hh_s \to \gamma\gamma b\bar{b})$, (d) $\sigma(gg \to H \to hh_s \to \tau\bar{\tau}b\bar{b})$, (e) $\sigma(gg \to A_H \to Zh \to Zb\bar{b})$, (f) $\sigma(gg \to A_H \to Zh_s \to \ell\ell b\bar{b})$, (g) $\sigma(gg \to H \to h_s h_s \to b\bar{b}b\bar{b})$, (h) $C_{Ht\bar{t}}$, and (i) $C_{A_Ht\bar{t}}$. Solid and dashed contours indicate the 1σ and 2σ credible regions, respectively. Colored diamonds denote the four benchmark points corresponding to those in Fig. 1, with details provided in Table 2 and Table 3.

approximately 68% and 23% of the total Bayesian evidence, respectively, indicating a clear preference of current experimental data for the former. The posterior PDF distributions of $\mu_{\gamma\gamma}$, $\mu_{b\bar{b}}$, and $\sigma(gg \to H \to hh_s \to \gamma\gamma b\bar{b})$ as functions of the heavy Higgs mass m_H are shown in the upper panels of Fig. 2. The solid contours indicate the 1σ credible regions. For 625 GeV $\lesssim m_H \lesssim 640$ GeV, we find:

$$0.16 \lesssim \mu_{\gamma\gamma} \lesssim 0.21$$
, $0.0 \lesssim \mu_{b\bar{b}} \lesssim 0.04$, $0.04 \text{ fb} \lesssim \sigma(gg \to H \to hh_s \to \gamma\gamma b\bar{b}) \lesssim 0.06 \text{ fb}$.

into a one-dimensional integral while sampling the parameter space [145–148]. The evidence integral can be written as [146]:

$$\mathcal{Z} = \int_0^1 \mathcal{L}(X) dX, \quad X(\lambda) = \int_{\mathcal{L}(\Theta)} \pi(\Theta) d^D\Theta,$$

where Θ is the input parameters of the model, D the dimensionality of the parameter space, $\pi(\Theta)$ the prior, $\mathcal{L}(\Theta)$ the likelihood, and X the 'prior volume' with the definition $dX = \pi(\Theta)d^D\Theta$.

For 640 GeV $\lesssim m_H \lesssim 675$ GeV, we find:

$$0.02 \lesssim \mu_{\gamma\gamma} \lesssim 0.09$$
, $0.14 \lesssim \mu_{b\bar{b}} \lesssim 0.25$, $0.07 \text{ fb} \lesssim \sigma(gg \to H \to hh_s \to \gamma\gamma b\bar{b}) \lesssim 0.105 \text{ fb}$.

As expected, **Scenario I** and **Scenario II** primarily populate the regions with $m_H \lesssim$ 640 GeV and $m_H \gtrsim$ 640 GeV, respectively. The pattern displayed in the $\mu_{\gamma\gamma} - m_H$ and $\mu_{b\bar{b}} - m_H$ planes can be understood from the fact that heavier mass of m_H requires an increasing $\text{Br}_{\text{SUSY}}(h_s \to b\bar{b})$ to keep $\sigma(gg \to H \to hh_s \to \gamma\gamma b\bar{b})$ from decreasing for kinematic reasons, thus leading to a higher $\mu_{b\bar{b}}$ and lower $\mu_{\gamma\gamma}$.

As mentioned earlier, the cross section $\sigma(gg \to H \to hh_s \to \tau \bar{\tau}b\bar{b})$ is constrained to be below about 3 fb for 600 GeV $\lesssim m_H \lesssim 700$ GeV by CMS [12]. Panel (d) of Fig. 2 shows that both the 1σ and 2σ credible regions lie well within the current experimental bounds.

We further explore several phenomenologically interesting search channels and present their prospects as tests of the model. The scenarios studied here predict a doublet–like CP–odd Higgs boson A_H with a mass range of 450 GeV $\lesssim m_{A_H} \lesssim 650$ GeV (corresponding to m_H varying from ~ 675 GeV to ~ 625 GeV) at the 1σ level. Searches in the channel $\sigma(gg \to A_H \to Zb \to Zb\bar{b})$ conducted by CMS [149] and ATLAS [150] place a 95% CL upper limit of roughly 30 fb near $m_{A_H} \simeq 600$ GeV (or equivalently $m_H \simeq 645$ GeV). This limit relaxes to about 100 fb as m_{A_H} decreases to 450 GeV (or m_H increases to 675 GeV). Searches in the complementary channel $\sigma(gg \to A_H \to Zh_s \to \ell\ell b\bar{b})$ by CMS [151] impose upper limits between 20 and 30 fb for 625 GeV $\lesssim m_H \lesssim 675$ GeV. Panels (e) and (f) of Fig. 2 display the corresponding predictions, demonstrating that they lie safely below the current bounds and are likely to be probed at future high–luminosity collider runs.

Considering that the decays of H or A_H into top-quark pairs may provide promising search channels, we show the normalized couplings $C_{Ht\bar{t}}$ and $C_{A_Ht\bar{t}}$ in panels (h) and (i) of Fig. 2, respectively. The CMS search for heavy resonances decaying into $t\bar{t}$ [152] sets an approximate upper limit of $C_{Ht\bar{t}} \simeq 0.86$ for the ratio of width to mass $\Gamma_H/m_H \simeq 2.5\%$, and $C_{A_Ht\bar{t}} \simeq 0.75$ for $\Gamma_{A_H}/m_{A_H} \simeq 2.5\%$ with $m_H \simeq 629$ GeV. It is worth noting that in panel (i) of Fig.2 the region with $C_{A_Ht\bar{t}} \lesssim 0.60$ corresponds entirely to **Scenario I**, while values above 0.6 correspond to **Scenario II**. The origin of this separation is clarified later in the discussion of the lower-left panel of Fig. 3.

We also calculate the cross sections of H decaying into the SM-like Higgs pairs $\sigma(gg \to H \to hh)$ and the light Higgs pairs $\sigma(gg \to H \to h_s h_s)$. The largest value in the 1σ region of $\sigma(gg \to H \to hh)$ is about 20 fb for **Scenario I** and 3.5 fb for **Scenario II**. For the $h_s h_s$ channel, this channel is significantly more promising, with the largest cross-section reaching 25 fb for Scenario I and a substantial 120 fb for Scenario II. The largest predicted values of $\sigma(gg \to H \to h_s h_s)$ multiplied by the relevant branching fractions into the final states $b\bar{b}b\bar{b}$, $b\bar{b}\tau\bar{\tau}$, and $b\bar{b}\gamma\gamma$ are approximately 36 fb, 4.5 fb and 0.23 fb, respectively. The distribution of the $\sigma(gg \to H \to h_s h_s \to b\bar{b}b\bar{b})$ cross-section is displayed in panel (g) of Figure 2.

Fig.3 shows the two-dimensional PL functions projected onto the (λ, κ) , (m_N, δ) ,

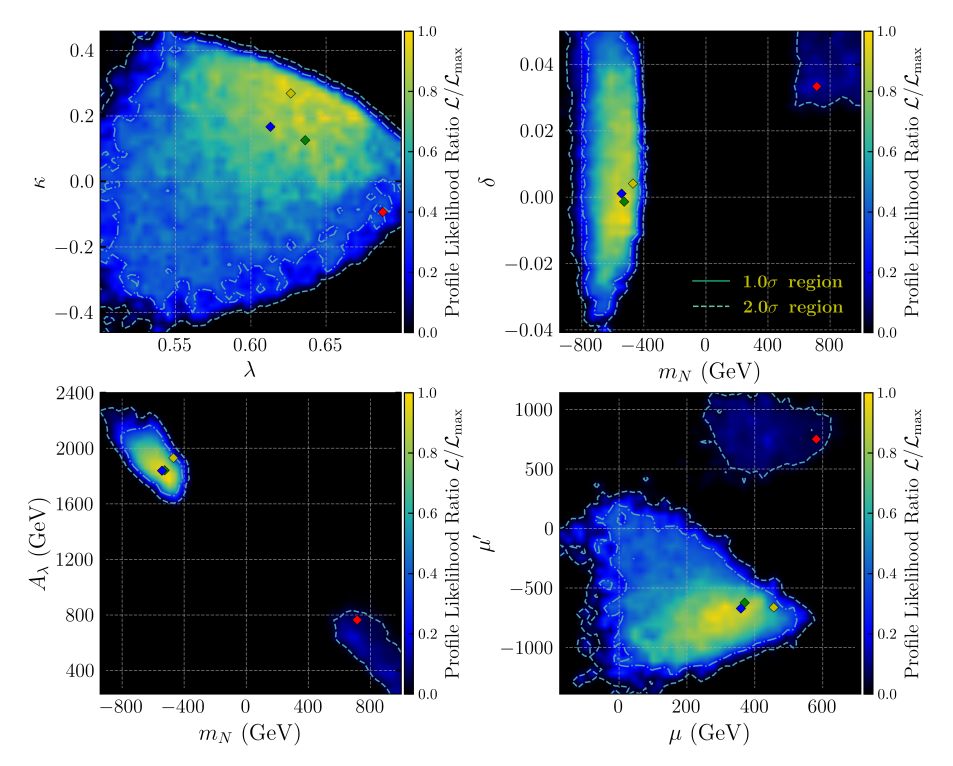


Figure 3. Two-dimensional profile likelihoods projected onto the (λ, κ) , (m_N, δ) , (m_N, A_λ) , and (μ, μ') planes. Dashed-dotted and dashed contours indicate the 1σ and 2σ confidence intervals, respectively. The best-fit point has a total χ^2 value of $\chi^2_{650+95} + \chi^2_{125} \simeq 162$. Colored diamonds denote the four benchmark points shown in Figs. 1 and 2.

 (m_N, A_λ) and (μ, μ') planes ⁴. The dashed-dotted and dashed contours delineate the 1σ and 2σ confidence intervals, respectively. The best-fit point yields a combined value of $\chi^2_{650+95} + \chi^2_{125} \simeq 162$. The upper-left panel shows that the 1σ regions of λ and κ span nearly the entire prior range, bounded only by the perturbativity condition. The preferred region lies at relatively large and positive values of (λ, κ) , where **Scenario I** and **Scenario II** overlap. In contrast, the remaining three panels reveal two clearly separated islands of viable solutions. We verify that

ScenarioI:
$$m_N \lesssim -390 \,\text{GeV}$$
, $A_{\lambda} \gtrsim 1600 \,\text{GeV}$, $\mu' \lesssim 400 \,\text{GeV}$,

while

ScenarioII:
$$m_N \gtrsim 550 \,\text{GeV}$$
, $A_{\lambda} \lesssim 800 \,\text{GeV}$, $\mu' \gtrsim 500 \,\text{GeV}$,

corresponding only to the 2σ credible region.

$$\mathcal{L}_{\text{prof}}(\theta_1, \theta_2) = \max_{\theta_3, \dots, \theta_n} \mathcal{L}(\theta_1, \theta_2, \theta_3, \dots, \theta_n).$$

At each point in the (θ_1, θ_2) plane, it represents the maximum likelihood compatible with the data after optimizing over all remaining nuisance parameters. The profile likelihood therefore encodes the maximally allowed parameter region consistent with current experimental data

⁴The two-dimensional profile likelihood for parameters (θ_1, θ_2) is defined as

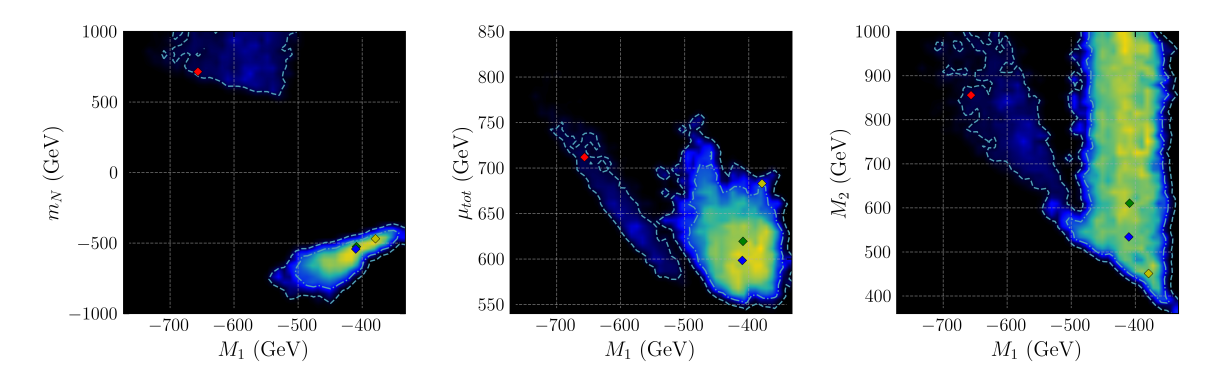


Figure 4. Same as Fig.3, but projected onto (M_1, m_N) , (M_1, μ_{tot}) , (M_1, M_2) planes.

The structure seen in the lower-left panel of Fig. 3 indicates that $A_{\lambda} + m_{N}$ is confined to nearly the same range in both scenarios. This behavior follows from the requirement that $A_{\lambda} + m_{N} \simeq 2\mu_{tot}$ (given $\tan \beta \simeq 1.6$), which is necessary to keep δ in the small range demanded by Eq. (2.5). Moreover, in **Scenario I**, the enhancement of $A_{\lambda} - m_{N}$ leads to a relatively larger mixing between $A_{\rm NSM}$ and A_{S} [see Eq. (2.4)], thereby suppressing the coupling of A_{H} to top-quark pairs. Conversely, in **Scenario II**, the partial cancellation between A_{λ} and m_{N} yields a larger $C_{A_{H}t\bar{t}}$, consistent with the pattern shown in panel (i) of Fig. 2. Finally, the (μ, μ') panel reveals 1σ and 2σ regions that significantly deviate from zero, suggesting that non-vanishing values of μ and μ' may serve as distinguishing features of the GNMSSM relative to the \mathbb{Z}_{3} -NMSSM and the MSSM.

Lastly, we discuss the DM dynamics relevant for explaining the observed excesses. Since both scenarios predict a Bino-dominated neutralino $\tilde{\chi}_1^0$ as the DM candidate, we show in Fig. 4 the PL functions of the Bino mass parameter M_1 correlated with the Singlino mass m_N , the total Higgsino mass parameter $\mu_{\rm tot}$, and the Wino mass M_2 . From the left panel of Fig. 4, one observes that the 1σ region of M_1 in Scenario I lies in the range $-500\,{\rm GeV} \lesssim M_1 \lesssim -300\,{\rm GeV}$. In this scenario, the relic density is obtained either through efficient s-channel resonance annihilation $\tilde{\chi}_1^0 \tilde{\chi}_1^0 \to h_s A_H$, which is enhanced when $2m_{\tilde{\chi}_1^0} \simeq m_{A_s} \simeq 800\,{\rm GeV}$, or through coannihilation with Singlino-dominated $\tilde{\chi}_2^0$ states. In the latter case, the dominant processes are $\tilde{\chi}_2^0 \tilde{\chi}_2^0, \tilde{\chi}_1^0 \tilde{\chi}_2^0 \to h_s A_H$, which together yield the correct DM abundance. In contrast, in Scenario II, the 2σ region favors heavier and more negative M_1 values $M_1 \lesssim -500\,{\rm GeV}$. As seen from the middle panel of Fig. 4, the relic density is predominantly controlled by coannihilation with Higgsino-dominated $\tilde{\chi}_2^0$ or $\tilde{\chi}_1^{\pm}$ states. The leading channels in this case are $\tilde{\chi}_1^+ \tilde{\chi}_1^-, \tilde{\chi}_2^0 \tilde{\chi}_2^0 \to h_s A_s$, as well as processes such as $\tilde{\chi}_1^+ \tilde{\chi}_2^0 \to u \bar{d}, h_s W^+$. These channels efficiently reduce the relic abundance to the observed level.

In Fig. 5, the SI and SD DM–nucleon scattering cross sections are shown as functions of the LSP mass $m_{\tilde{\chi}_1^0}$ in the left and right panels, respectively. For comparison, we overlay the latest 90% CL upper limits from the combined WS2024+WS2022 analysis of the LZ experiment [127, 128], the projected sensitivities for future LZ runs [153], and the expected neutrino background [154]. The left panel illustrates that most viable samples lie well below

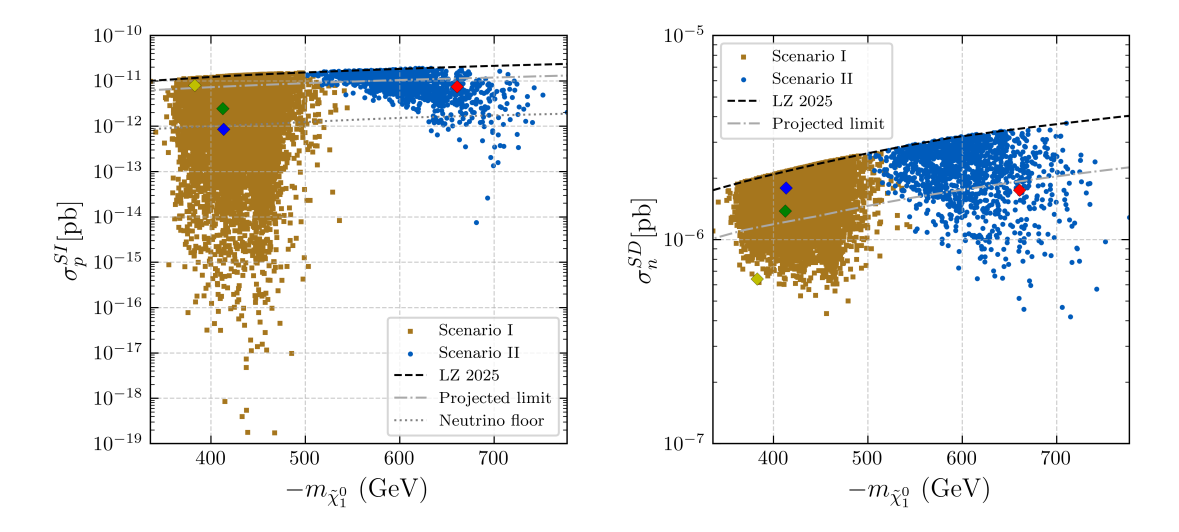


Figure 5. Spin-independent (SI) and spin-dependent (SD) DM-nucleon scattering cross sections, $\sigma_p^{\rm SI}$ (left) and $\sigma_n^{\rm SD}$ (right), as functions of the LSP mass $m_{\tilde{\chi}_1^0}$. Dashed black lines show the 90% C.L. upper limits from the 2025 LZ results [127, 128], dashed-dotted grey lines indicate the projected LZ sensitivities for future runs [153], and dotted lines denote the neutrino floor [154]. Amber squares and blue dots correspond to **Scenario I** and **Scenario II**, respectively. Colored diamonds represent the four benchmark points shown in Figs. 1–4.

both the current and projected SI limits. Within **Scenario I**, samples with $\sigma(gg \to H \to hh_s \to \gamma\gamma b\bar{b}) > 0.09$ fb in the lower $m_{\tilde{\chi}1^0}$ region generally predict smaller $\sigma_p^{\rm SI}$ compared with **Scenario II**, whose points satisfying $\chi^2_{\sigma\gamma\gamma b\bar{b}} + \chi^2_{\mu_{rr}} \leq 6.18$ appear at larger $m_{\tilde{\chi}_1^0}$. The right panel shows that while all samples remain consistent with current SD bounds, the projected sensitivity can probe roughly half of them.

To further clarify the model's interpretation of the observed excesses, four benchmark points—P1, P2, and P3 from **Scenario I**, and P4 from **Scenario II**—are selected to illustrate representative behaviors. These benchmarks, highlighted as blue, yellow, green, and red diamonds in all figures, are listed with full details in Tables 2 and 3. P1 and P2 simultaneously account for the $\sigma_{\gamma\gamma b\bar{b}}$ and μ_{rr} excesses at the 2σ level, while P3 explains the combined excesses of $\sigma_{\gamma\gamma b\bar{b}}$ and $\mu_{b\bar{b}}$ at the same significance. P4 provides a 2σ interpretation of the combined $\sigma_{\gamma\gamma b\bar{b}}$ and μ_{rr} anomalies. The DM in P1 predominantly annihilates via the A_s -funnel into $h_s A_H$, whereas in P2 and P3 the relic abundance is mainly obtained through coannihilation with Singlino-dominated $\tilde{\chi}_2^0$ into $h_s A_H$. P1 may be probed by future SD searches, but its SI cross section is suppressed to near the neutrino floor due to the blind-spot condition $\sin 2\beta + m_{\tilde{\chi}_1^0}/\mu \simeq 0.002$, which reduces the Higgs-exchange contribution. P2, on the other hand, predicts extremely low SD neutron cross section (as low as 6.5×10^{-7} pb), owing to the heavy suppression of the $\tilde{\chi}_1^0$ -Z gauge boson coupling, driven by $N_{13}^2 - N_{14}^2 \simeq 0.004$.

Regarding constraints from the LHC searches for SUSY, simulation results of electroweakino productions, utilizing the package CheckMATE-2.0.26, consistently indicate

that the constraints from LHC searches for new physics are minimal. The calculated R-values for all benchmark points are less than 0.35, confirming that the parameter space is safely compliant with existing 95% CL limits. The basic reason for these weak restrictions is that the interpretation of the scalar excesses primarily relies on Higgs sector mixing effects rather than sizable contributions from loop effects involving light SUSY particles. Specific analysis of the benchmark points highlights the dominant search channels:

- P1 and P3: The most significant signal region is G05 from the CMS report CMS-SUS-16-039 [155]. This targets events with at least four leptons, no τ leptons, and high missing transverse momentum ($p_T^{\text{miss}} \geq 200 \text{ GeV}$).
- P2: This point is most sensitive to the off-shell WZ selection from the ATLAS report ATLAS-2106-01676 [156], which requires at least one jet and high p_T^{miss} .
- P4: This point yields the lowest R value because it predicts a highly compressed mass spectrum, with a mass difference $\Delta m(\tilde{\chi}_2^0, \tilde{\chi}_1^0) \lesssim 20$ GeV, making the decay products too soft to be effectively detected by current searches.

For each benchmark, the most significant signal regions, corresponding R values, and the associated experimental analyses are precisely listed in the bottom row of Table. 2 and Table. 3.

4 Conclusion

The $\mu_{\gamma\gamma}$ excess reported by CMS and ATLAS and the $\mu_{b\bar{b}}$ excess observed at LEP hint in a compatible way at the existence of a light Higgs boson near 95 GeV. In parallel, an excess in the resonant production of SM-like plus BSM Higgs bosons in the diphoton plus bb channel by CMS suggests an extra heavy Higgs bosons near 650 GeV. This research rigorously investigated the capacity of the GNMSSM to simultaneously explain the 95 GeV and 650 GeV excesses while providing a proper DM candidate with correct DM relic abundance. We adopt a framework in which the light singlet-like CP-even Higgs boson h_s accounts for the the 95 GeV anomalies, whereas the heavy doublet-like CP-even Higgs boson H decays into the SM-like Higgs h and h_s to account for the $\sigma_{\gamma\gamma b\bar{b}}$ excess. This configuration, characterized by small $\tan \beta$ and large λ , is theoretically well-motivated as it leverages the tree-level singlet-doublet mixing to elevate the mass of the 125 GeV Higgs boson (h) without relying on excessively large radiative corrections. To streamline the parameterization, a small auxiliary factor δ is introduced, which substantially improves sampling efficiency without affecting the underlying physics. By performing a comprehensive 12-dimensional parameter scan using state-of-the-art sampling and numerical tools, constrained by a battery of experimental limits including 125 GeV Higgs data, B-physics, vacuum stability, and the most stringent LZ Dark Matter results, we successfully demonstrated the model's viability. The key findings and insights derived from this analysis are summarized below::

Table 2. Details of the benchmark points P1 and P2 from **Scenario I**, represented as blue and yellow diamonds, respectively, in all figures. Both points can account for the di-photon and $b\bar{b}$ excesses near 95 GeV, as well as the $\sigma_{\gamma\gamma b\bar{b}}$ excess at the 2σ level, while satisfying all applied constraints. Here, d_i and u_i in the annihilation final states denote the *i*th generation of down-type and up-type quarks, respectively.

Benchmark Point P1			Benchmark Point P2						
μ_{tot}	$598.4~{ m GeV}$	λ	0.613	μ_{tot}	682.9 GeV	λ			0.627
μ	$359.4~{ m GeV}$	κ	0.167	μ	$456.3~\mathrm{GeV}$	κ			0.269
μ'	$-672.4 \mathrm{GeV}$	δ	0.001	μ'	$-663.4 \mathrm{GeV}$	δ			0.004
M_1	$-409.8 \mathrm{GeV}$	$\tan \beta$	1.501	M_1	$-379.1 \mathrm{GeV}$	$\tan \beta$			1.465
M_2	$533.8~{ m GeV}$	A_{λ}	$1838~{ m GeV}$	M_2	$450.9~\mathrm{GeV}$	A_{λ}			$1930~{\rm GeV}$
m_A	$623.6~\mathrm{GeV}$	A_{κ}	$1762~{ m GeV}$	m_A	$639.4~{ m GeV}$	A_{κ}			$1640~{\rm GeV}$
m_B	$93.68~{ m GeV}$	A_t	$1646~{ m GeV}$	m_B	$103.4~{\rm GeV}$	A_t			$1619~{\rm GeV}$
m_N	-542.7 GeV			m_N	$-469.3 \mathrm{GeV}$				
$m_{{ ilde \chi}_1^0}$	-413.5 GeV	m_{h_s}	94.70 GeV	$m_{\tilde{\chi}_1^0}$	-382.9 GeV	m_{h_s}			95.17 GeV
$m_{{ ilde \chi}_2^0}$	$-461.4 \mathrm{GeV}$	m_h	$127.4~{ m GeV}$	$m_{\tilde{\chi}_2^0}$	$420.1~\mathrm{GeV}$	m_h			$127.4~{ m GeV}$
$m_{\tilde{\chi}^0_2}$	502.6 GeV	m_H	$654.4~{ m GeV}$	$m_{\tilde{\chi}^0_3}$	$450.0~{\rm GeV}$	m_H			$670.6~\mathrm{GeV}$
$m_{ ilde{\chi}^0_4}$	$660.5~\mathrm{GeV}$	m_{A_s}	$493.5~\mathrm{GeV}$	$m_{\tilde{\chi}^0_4}$	$713.5~{ m GeV}$	m_{A_s}			503.2 GeV
$m_{\tilde{\chi}_{5}^{0}}$	$-675.6 \mathrm{GeV}$	m_{A_H}	$875.3~\mathrm{GeV}$	$m_{\tilde{\chi}_{\rm g}^0}$	-728.6 GeV	m_{A_H}			$886.3~{\rm GeV}$
$m_{\tilde{\chi}_1^{\pm}}$	$502.0~{ m GeV}$	$m_{H^{\pm}}$	$637.9~\mathrm{GeV}$	$m_{\tilde{\chi}_1^{\pm}}^{\lambda_5}$	$450.0~{\rm GeV}$	$m_{H^{\pm}}$			654.1 GeV
$m_{\tilde{\chi}^{\pm}_{0}}^{\chi_{1}}$	$659.5~\mathrm{GeV}$	11		$m_{\tilde{\chi}_{0}^{\pm}}^{\chi_{1}}$	$712.0~{ m GeV}$	11			
$\frac{\chi_2}{\Omega h^2}$	***************************************	0.138		Ωh^2	,-=	0.111			
σ_p^{SI} , σ_n^{SD}		$8.4 \times 10^{-49} \text{ cm}^2$, 1.	$7 \times 10^{-42} \text{ cm}^2$	σ_p^{SI} , σ_n^{SD}		7.9×10^{-48} cm	$a^2 - 6.4 \times 1$	0^{-43} c	m^2
$\frac{\sigma_p}{\mu_{\gamma\gamma}}$, σ_n		0.081	7 × 10 Cm	$\mu_{\gamma\gamma}$		0.081	1 , 0.4 × 1	.0 0	111
$\mu_{b\bar{b}}$		0.229		$\mu_{b\bar{b}}$		0.230			
$\sigma_{\gamma\gamma b\bar{b}}$		0.091 fb		$\sigma_{\gamma\gamma b\bar{b}}$		0.092 fb			
$\sigma(gg \rightarrow H \rightarrow hh$	$a \rightarrow \tau \bar{\tau} b \bar{b}$	1.889 fb		$\sigma \gamma \gamma_{bb} \over \sigma (gg \rightarrow H \rightarrow hh_s \rightarrow hh_$	$\tau \bar{\tau} b \bar{b}$)	1.898 fb			
$\sigma(gg \to H \to h_s)$		0.177 fb		$\sigma(gg \to H \to h_s h_s h_s h_s h_s h_s \to h_s h_s h_s h_s h_s h_s h_s h_s h_s h_s$		0.395 fb			
$\sigma(gg \to A_H \to Z)$		7.878 fb		$\sigma(gg \to A_H \to Zh \to Z$		7.693 fb			
$\sigma(gg \to A_H \to Z)$		8.146 fb		$\sigma(gg \to A_H \to Zh_s -$		7.600 fb			
	$C_{h_s\gamma\gamma}$, $C_{h_s t\bar{t}}$, $C_{h_s b\bar{b}}$	0.385, 0.459, 0.4	37, 0.382, 0.631	C_{h_sqq} , C_{h_sVV} , $C_{h_s\gamma\gamma}$		0.383, 0.461,	0.442,	0.380,	0.633
	$C_{h\gamma\gamma}$, $C_{ht\bar{t}}$, $C_{hb\bar{b}}$		15, 0.921, 0.815	C_{hqq} , C_{hVV} , $C_{h\gamma\gamma}$,		0.929, 0.888,			0.813
	$C_{H\gamma\gamma}$, $C_{Ht\bar{t}}$, $C_{Hb\bar{b}}$	0.580, 0.009, 4.2		C_{Hqq} , C_{HVV} , $C_{H\gamma}$		0.592, 0.009,		0.686,	1.444
	, $C_{A_H t \bar{t}}$, $C_{A_H b \bar{b}}$	0.686, 1.157, 0.5		$C_{A_H gg}$, $C_{A_H \gamma \gamma}$, C_A	,	0.676, 1.243,		1.189	
$N_{11}, N_{12}, N_{13},$		0.990, -0.001, 0.0	96, 0.040, -0.092	N ₁₁ , N ₁₂ , N ₁₃ , N ₁₄ ,	N ₁₅	0.993, 0.002	. 0.070.	0.016,	-0.099
$N_{21}, N_{22}, N_{23},$		-0.130, 0.010, 0.3	392, 0.423, -0.806	N ₂₁ , N ₂₂ , N ₂₃ , N ₂₄ ,		-0.113, 0.008	, 0.240,	-0.270,	-0.926
N_{31} , N_{32} , N_{33} ,		-0.027, -0.809, 0.4	23, -0.406, -0.013	N ₃₁ , N ₃₂ , N ₃₃ , N ₃₄ ,		0.015, 0.954	, -0.221,	0.202,	0.008
N_{41} , N_{42} , N_{43} ,	N_{44}, N_{45}	0.033, -0.587, -0.5	667, 0.576, 0.013	N_{41} , N_{42} , N_{43} , N_{44} ,	N_{45}	-0.038, 0.300	, 0.672,	-0.675,	-0.016
N_{51} , N_{52} , N_{53} ,	N_{54}, N_{55}	0.025, -0.010, -0.5	579, -0.568, -0.584	N_{51} , N_{52} , N_{53} , N_{54} ,	N_{55}	0.021, -0.011	, -0.661,	-0.655,	-0.365
Annihilations		Fractions [%]		Annihilations		Fractions [%]			
$\tilde{\chi}_1^0 \tilde{\chi}_1^0 \rightarrow h_s A_H / I$	$H^{\pm}W^{\mp}/t\bar{t}/HZ/h_sZ$	23/20/15/6.9/1.0		$\tilde{\chi}_{2}^{0}\tilde{\chi}_{2}^{0} \rightarrow h_{s}A_{H}/H^{\pm}W$	$r^{\mp}/t\bar{t}/HZ/h_sZ$	31/24/12/8.3	/2.3		
$\tilde{\chi}_1^0 \tilde{\chi}_2^0 \rightarrow H^{\pm} W^{\mp}$	$/h_sA_H/HZ/t\bar{t}$	11/8.3/3.8/3.7		$\tilde{\chi}_{1}^{0}\tilde{\chi}_{2}^{0} \rightarrow h_{s}A_{H}/t\bar{t}/H^{\pm}$	$\pm W^{\mp}$	4.8/2.8/2.8			
$\tilde{\chi}_{2}^{0}\tilde{\chi}_{2}^{0} \rightarrow t\bar{t}/h_{s}A_{F}$	Y	1.2/1.0		$\tilde{\chi}_1^0 \tilde{\chi}_1^0 \rightarrow h_s A_H / t\bar{t}$		2.6/1.6			
Decays		Branching ratios [%]	Decays		Branching rat	ios [%]		
$\tilde{\chi}_1^0 \tilde{\chi}_2^0 \rightarrow H^{\pm} W^{\mp}$	$/h_sA_H/t\bar{t}/HZ$	17/11/7.0/6.7			$/hW^-/A_sW^-/A_HW^-$	11/4.4/2.9/2.9	0/1.6		
$\tilde{\chi}_1^0 \tilde{\chi}_1^0 \rightarrow h_s A_H / I$	$H^{\pm}W^{\mp}/t\bar{t}/HZ$	9.1/8.8/8.1/3.4		$\tilde{\chi}_{2}^{0}\tilde{\chi}_{2}^{0} \rightarrow h_{s}A_{H}/HZ/t$	$t\bar{t}/W^+W^-$	5.7/1.7/1.6/1.	5		
$\tilde{\chi}_{2}^{0}\tilde{\chi}_{2}^{0} \rightarrow h_{s}A_{H}/t$	\bar{t}	5.9/5.6		$\tilde{\chi}_{1}^{\pm} \tilde{\chi}_{1}^{\mp} \rightarrow h_{s} A_{H} / W^{+} I$	$W^-/t\bar{t}$	4.8/1.4/1.3			
Decays		Branching ratios [%]	Decays		Branching rat	ios [%]		
	$c\bar{c}/gg/W^+W^{-*}/\gamma\gamma$	87.2/9.65/1.51/1.42	/0.09/0.08	$h_s \rightarrow b\bar{b}/\tau^+\tau^-/c\bar{c}/gg$	$\eta/W^+W^{-*}/\gamma\gamma$	87.2/9.66/1.49	9/1.41/0.10	0/0.08	
$h \rightarrow b\bar{b}/W^+W^{-*}/\tau^+\tau^-/gg/ZZ/c\bar{c}/\gamma\gamma$ 51.7		51.7/30.0/6.02/5.47/3.42/3.11/0.029		$h \rightarrow b\bar{b}/W^+W^{-*}/\tau^+$	$\tau^{-}/gg/ZZ/c\bar{c}/\gamma\gamma$	51.6/30.0/6.01	/5.51/3.43	3/3.14/	0.029
$H \to t\bar{t}/A_H Z/hh_s/hh$ 67.8/18.9/8.26/4.63			$H \to t\bar{t}/A_H Z/hh_s/hh$ 66.6/19.1/8.99/4.96		9/4.96				
$A_H \rightarrow t\bar{t}/h_s Z/h$		94.7/4.27/0.70		$A_H \rightarrow t\bar{t}/h_s Z/hZ$		94.4/4.43/0.76			
$A_s \to H^{\pm}W^{\mp}/h_s A_H/t\bar{t}/h_s Z$ 36.9/29.0/17.2/13.7			$A_s \rightarrow h_s A_H / H^{\pm} W^{\mp}$, ,	33.7/ 31.7/16.7/11.6				
$H^+ \rightarrow t\bar{b}/A_sW^+$	$^+/h_sW^+/hW^+$	76.8/15.1/6.93/1.19		$H^+ \rightarrow t\bar{b}/A_sW^+/h_sV$	W^+/hW^+	75.8/15.7/7.21	/1.29		
$\tilde{\chi}^0_2 \rightarrow \tilde{\chi}^0_1 Z^*$		100		$\tilde{\chi}_2^0 \rightarrow \tilde{\chi}_1^0 Z^*$		100			
$\tilde{\chi}^0_3 \rightarrow \tilde{\chi}^0_1 Z / \tilde{\chi}^0_2 Z$	-T O O -	76.6/23.3		$\tilde{\chi}_3^0 \rightarrow \tilde{\chi}_1^0 Z / \tilde{\chi}_2^0 Z$	0 0-	68.4/31.6	4		
$\tilde{\chi}_4^0 \rightarrow \tilde{\chi}_2^0 Z/\tilde{\chi}_1^{\pm} W$		43.1/42.0/6.59/2.28		$\tilde{\chi}_4^0 \rightarrow \tilde{\chi}_1^{\pm} W^{\mp}/\tilde{\chi}_2^0 Z/\tilde{\chi}_2^0$		40.7/39.2/17.8	,		
$\tilde{\chi}_5^0 \rightarrow \tilde{\chi}_2^{\pm} W^{\mp}/\tilde{\chi}_3^0$	$\frac{1}{3}Z/\tilde{\chi}_{2}^{0}h/\tilde{\chi}_{2}^{0}h_{s}$	46.9/20.3/17.5/13.1		$\tilde{\chi}_{5}^{0} \rightarrow \tilde{\chi}_{2}^{\pm}W^{\mp}/\tilde{\chi}_{2}^{0}h/\tilde{\chi}_{5}^{0}$	$\frac{G}{3}Z/\tilde{\chi}_{2}^{0}h_{s}$	41.8/35.0/19.7	7/1.85		
$\tilde{\chi}_1^+ \rightarrow \tilde{\chi}_1^0 W^{+*}$	Draw Land of the Land	100		$\tilde{\chi}_1^+ \rightarrow \tilde{\chi}_1^0 W^{+*}$	rat grati	100			
$\tilde{\chi}_2^+ \rightarrow \tilde{\chi}_2^0 W^+/\tilde{\chi}_3^0$	$\langle W^+/\tilde{\chi}_1^+Z/\tilde{\chi}_1^+h \rangle$	43.4/22.7/18.9/6.58		$\tilde{\chi}_{2}^{+} \rightarrow \tilde{\chi}_{2}^{0}W^{+}/\tilde{\chi}_{3}^{0}W^{+}$	$/\chi_1^+ Z/\tilde{\chi}_1^+ h$	38.4/21.2/20.2	2/18.0		
R value		0.15		R value		0.22			
Signal Region		G05 in CMS-SUS-1		Signal Region		$SR_{high}^{offWZ} - nj$			

- 1. The best fit in **Scenario I** provides a simultaneous interpretation of the $\sigma_{\gamma\gamma b\bar{b}}$ excess near 650 GeV and μ_{rr} and $\mu_{b\bar{b}}$ excesses near 95 GeV at the 2σ level. Larger values of $\sigma_{\gamma\gamma b\bar{b}}\gtrsim 0.1$ fb are limited by the CMS search in the $\tau\bar{\tau}$ plus $b\bar{b}$ channel.
- 2. **Scenario II** successfully combines the $\sigma_{\gamma\gamma b\bar{b}}$ and $\mu_{\gamma\gamma}$ excesses at the 2σ level, with $\mu_{\gamma\gamma}$ achieving its central value while $\mu_{b\bar{b}}$ remains within the 2σ range.

Table 3. Details of the benchmark points P3 from **Scenario I** and P4 from **Scenario II**, represented as green and red diamonds, respectively, in all figures. P3 can simultaneously account for the $\sigma_{\gamma\gamma b\bar{b}}$ and $\mu_{b\bar{b}}$ excesses at the 2σ level, while P4 can describe the combined excesses of $\sigma_{\gamma\gamma b\bar{b}}$ and μ_{rr} at the 2σ level.

Benchr	nark Point P3	Benchmark Point P4			
μ_{tot} 619.3 G	V λ 0.636	μ_{tot} 711.8 GeV	λ 0.688		
μ 370.3 G	eV κ 0.125	μ 581.5 GeV	κ -0.094		
μ' -624.0 G	eV δ -0.001	μ' 750.4 GeV	δ 0.033		
M_1 -408.8 G	eV $\tan \beta$ 1.413	M_1 -656.4 GeV	$\tan \beta$ 1.467		
M_2 610.3 G	$V A_{\lambda}$ 1841 GeV	M_2 855.4 GeV	A_{λ} 763.8 GeV		
m_A 629.6 G	$V A_{\kappa}$ 1656 GeV	m_A 1552 GeV	A_{κ} -1955 GeV		
m_B 95.18 G	$V A_t$ 1413 GeV	m_B 97.57 GeV	A_t 1082 GeV		
m_N -525.8 G	·V	m_N 714.9 GeV			
$m_{\tilde{\chi}_{1}^{0}}$ -412.7 Ge	$PV = m_{h_s}$ 94.81 GeV	$m_{\tilde{\chi}_{1}^{0}}$ -660.9 GeV	m_{h_s} 95.37 GeV		
$m_{\tilde{\chi}_{2}^{0}}$ -451.8 G	$eV = m_h$ 123.6 GeV	$m_{\tilde{\chi}_{2}^{0}}$ 679.0 GeV	m_h 127.3 GeV		
$m_{\tilde{\chi}_{3}^{0}}$ 554.8 G	$eV m_H$ 647.8 GeV	$m_{\tilde{\chi}_{2}^{0}}^{2}$ -728.8 GeV	m_H 629.0 GeV		
$m_{\tilde{\chi}_{4}^{0}}^{3}$ -688.4 Ge	$W = m_{A_s}$ 484.3 GeV	$m_{\tilde{\chi}_{4}^{0}}^{3}$ 730.3 GeV	m_{A_s} 615.6 GeV		
$m_{\tilde{\chi}_{E}^{0}}^{^{^{^{^{^{^{^{^{^{^{^{^{^{^{^{^{$	m_{A_H} 884.8 GeV	$m_{\tilde{\chi}_{5}^{0}}^{^{-4}}$ 913.3 GeV	m_{A_H} 809.9 GeV		
$m_{\tilde{\chi}_{\pm}^{\pm}}^{^{5}}$ 553.8 G	$eV = m_{H^{\pm}}$ 635.3 GeV	$m_{\tilde{\chi}_{1}^{\pm}}^{5}$ 688.9 GeV	$m_{H^{\pm}}$ 617.9 GeV		
$m_{\tilde{\chi}_{\alpha}^{\pm}}^{\chi_1}$ 706.4 Ge		$m_{\tilde{\chi}_{2}^{\pm}}^{\chi_{1}}$ 913.1 GeV			
$\frac{\chi_2}{\Omega h^2}$	0.107	Ωh^2	0.114		
σ_p^{SI} , σ_n^{SD}	$2.4 \times 10^{-48} \text{ cm}^2$, $1.4 \times 10^{-42} \text{ cm}^2$	σ_n^{SI} , σ_n^{SD}	$7.4 \times 10^{-48} \text{ cm}^2, 1.7 \times 10^{-42} \text{ cm}^2$		
$\mu_{\gamma\gamma}$	0.057	$\mu_{\gamma\gamma}$	0.195		
$\mu_{bar{b}}$	0.178	$\mu_{bar{b}}$	0.014		
$\sigma_{\gamma\gamma bar{b}}$	0.099 fb	$\sigma_{\gamma\gamma bar{b}}$	0.045 fb		
$\sigma(qq \rightarrow H \rightarrow hh_s \rightarrow \tau \bar{\tau} b\bar{b})$	2.398 fb	$\sigma(qq \rightarrow H \rightarrow hh_s \rightarrow \tau \bar{\tau} b\bar{b})$	1.262 fb		
$\sigma(gg \to H \to h_s h_s \to b\bar{b}b\bar{b})$	1.489 fb	$\sigma(gg \to H \to h_s h_s \to b\bar{b}b\bar{b})$	36.75 fb		
$\sigma(qq \rightarrow A_H \rightarrow Zh \rightarrow Zb\bar{b})$	5.364 fb	$\sigma(qq \to A_H \to Zh \to Zb\bar{b})$	0.579 fb		
$\sigma(gg \rightarrow A_H \rightarrow Zh_s \rightarrow llb\bar{b})$	7.616 fb	$\sigma(gg \to A_H \to Zh_s \to llb\bar{b})$	0.966 fb		
C_{h_sgg} , C_{h_sVV} , $C_{h_s\gamma\gamma}$, $C_{h_st\bar{t}}$, $C_{h_sb\bar{b}}$	0.330, 0.404, 0.378, 0.328, 0.557	C_{h_aqq} , C_{h_aVV} , $C_{h_a\gamma\gamma}$, $C_{h_st\bar{t}}$, $C_{h_sb\bar{b}}$	0.280, 0.145, 0.172, 0.254, 0.089		
C_{hqq} , C_{hVV} , $C_{h\gamma\gamma}$, $C_{ht\bar{t}}$, $C_{hb\bar{b}}$	0.949, 0.915, 0.939, 0.940, 0.863	C_{hgg} , C_{hVV} , $C_{h\gamma\gamma}$, $C_{ht\bar{t}}$, $C_{hb\bar{b}}$	0.967, 0.989, 1.006, 0.966, 1.039		
C_{Hqq} , C_{HVV} , $C_{H\gamma\gamma}$, $C_{Ht\bar{t}}$, $C_{Hb\bar{t}}$	0.618, 0.010, 4.619, 0.713, 1.394	C_{Hqq} , C_{HVV} , $C_{H\gamma\gamma}$, $C_{Ht\bar{t}}$, $C_{Hb\bar{b}}$	0.593, 0.011, 4.530, 0.683, 1.437		
$C_{A_H gg}$, $C_{A_H \gamma \gamma}$, $C_{A_H t \bar{t}}$, $C_{A_H b \bar{b}}$	0.731, 1.137, 0.581, 1.161	$C_{A_H gg}$, $C_{A_H \gamma \gamma}$, $C_{A_H t \bar{t}}$, $C_{A_H b \bar{b}}$	0.745, 4.688, 0.681, 1.467		
N ₁₁ , N ₁₂ , N ₁₃ , N ₁₄ , N ₁₅	0.991, -0.002, 0.089, 0.032, -0.099	N ₁₁ , N ₁₂ , N ₁₃ , N ₁₄ , N ₁₅	-0.992, 0.000, -0.108, -0.064, -0.001		
N_{21} , N_{22} , N_{23} , N_{24} , N_{25}	0.128, 0.008, 0.353, 0.382, -0.844	N_{21} , N_{22} , N_{23} , N_{24} , N_{25}	-0.113, -0.027, -0.317, -0.613, 0.452		
N_{31} , N_{32} , N_{33} , N_{34} , N_{35}	-0.032, -0.691, 0.516, -0.504, -0.013	N_{31} , N_{32} , N_{33} , N_{34} , N_{35}	-0.122, 0.010, 0.698, 0.702, 0.008		
N_{41} , N_{42} , N_{43} , N_{44} , N_{45}	0.021, -0.008, -0.605, -0.597, -0.526	N_{41} , N_{42} , N_{43} , N_{44} , N_{45}	-0.012, -0.200, 0.340, -0.237, -0.888		
N_{51} , N_{52} , N_{53} , N_{54} , N_{55}	0.027, -0.722, -0.484, 0.493, 0.010	N_{51} , N_{52} , N_{53} , N_{54} , N_{55}	0.010, -0.927, -0.260, 0.268, 0.038		
Annihilations	Fractions [%]	Annihilations	Fractions [%]		
$\tilde{\chi}_1^0 \tilde{\chi}_2^0 \rightarrow H^{\pm} W^{\mp}/h_s A_H/t\bar{t}/HZ$	17/11/7.0/6.7	$\tilde{\chi}_{2}^{0}\tilde{\chi}_{1}^{-} \rightarrow d_{i}\bar{u}_{i}/h_{s}W^{-}/hW^{-}/A_{s}W^{-}/A_{H}W^{-}$	11/4.4/2.9/2.9/1.6		
$\tilde{\chi}_1^0 \tilde{\chi}_1^0 \rightarrow h_s A_H / H^{\pm} W^{\mp} / t \bar{t} / H Z$	9.1/8.8/8.1/3.4	$\tilde{\chi}_{2}^{0}\tilde{\chi}_{2}^{0} \rightarrow h_{s}A_{H}/HZ/t\bar{t}/W^{+}W^{-}$	5.7/1.7/1.6/1.5		
$\tilde{\chi}_{2}^{0}\tilde{\chi}_{2}^{0} \rightarrow h_{s}A_{H}/t\bar{t}$	5.9/5.6	$\tilde{\chi}_{1}^{\pm}\tilde{\chi}_{1}^{\mp} \rightarrow h_{s}A_{H}/W^{+}W^{-}/t\bar{t}$	4.8/1.4/1.3		
Decays	Branching ratios [%]	Decays	Branching ratios [%]		
$h_s \rightarrow b\bar{b}/\tau^+\tau^-/c\bar{c}/gg/W^+W^{-*}/\gamma\gamma$	87.3/9.66/1.43/1.34/0.10/0.08	$h_s \rightarrow b\bar{b}/gg/c\bar{c}/\tau^+\tau^-/W^+W^{-*}/\gamma\gamma$	51.4/22.5/19.7/5.69/0.37/0.36		
$h \rightarrow b\bar{b}/W^+W^{-*}/\tau^+\tau^-/gg/c\bar{c}/ZZ/\tau^-$	$\gamma \gamma = 59.7/21.9/6.91/5.53/3.34/2.27/0.29$	$h \rightarrow b\bar{b}/W^+W^{-*}/\tau^+\tau^-/gg/ZZ/c\bar{c}/\gamma\gamma$	57.9/25.7/6.74/4.10/2.91/2.36/0.31		
$H \rightarrow t \bar{t}/A_H Z/h h_s/h h$	70.4/18.3/7.6/3.02	$H \rightarrow t\bar{t}/h_sh_s/hh$	67.8/25.1/6.58/0.20		
$A_H ightarrow t ar{t}/h_s Z/h Z$	96.1/3.26/0.34	$A_H \rightarrow t\bar{t}/h_s Z/h Z$	87.5/11.7/0.51		
$A_s \rightarrow H^{\pm}W^{\mp}/h_sA_H/t\bar{t}/h_sZ$	39.5/23.9/18.1/2.25	$A_s \rightarrow h_s A_H / H^{\pm} W^{\mp} / t \bar{t} / h A_H$	39.6/20.9/18.7/8.56		
$H^+ \to t\bar{b}/A_s W^+/h_s W^+/h W^+$ 78.1/15.8/5.48/0.59		$H^+ \rightarrow t\bar{b}/h_sW^+/hW^+$	85.9/13.5/0.59		
$\tilde{\chi}^0_2 \rightarrow \tilde{\chi}^0_1 Z^*$	100	$\tilde{\chi}_2^0 \rightarrow \tilde{\chi}_1^0 Z^*$	100		
$\tilde{\chi}_{3}^{0} \to \tilde{\chi}_{2}^{0} Z / \tilde{\chi}_{1}^{0} Z / \tilde{\chi}_{1}^{0} h$ $76.1/21.8/1.35$		$\tilde{\chi}_3^0 \rightarrow \tilde{\chi}_2^0 Z / \tilde{\chi}_1^{\pm} W^{\mp} / \tilde{\chi}_1^0 Z$	49.8/48.6/3.13		
$\tilde{\chi}_{0}^{4} \rightarrow \tilde{\chi}_{1}^{\pm} W^{\mp} / \tilde{\chi}_{2}^{0} \tilde{\chi}_{2}^{0} / \tilde{\chi}_{3}^{0} Z / \tilde{\chi}_{2}^{0} h_{s}$ 39.1/31.8/14.4/11.8		$\tilde{\chi}_1^0 \rightarrow \tilde{\chi}_1^{\pm} W^{\mp}/\tilde{\chi}_1^0 h_s/\tilde{\chi}_2^0 Z$	69.7/15.6/5.80		
$\tilde{\chi}_{5}^{0} \to \tilde{\chi}_{2}^{\pm} W^{\mp} / \tilde{\chi}_{1}^{\pm} W^{\mp} / \tilde{\chi}_{3}^{0} h_{s} / \tilde{\chi}_{1}^{0} Z$ 49.3/35.6/11.9/1.9		$\tilde{\chi}_5^0 \rightarrow \tilde{\chi}_2^{\pm} W^{\mp}/\tilde{\chi}_3^0 Z/\tilde{\chi}_2^0 h/\tilde{\chi}_1^0 h_s$	55.7/16.7/15.9/6.61		
$\tilde{\chi}_1^+ \rightarrow \tilde{\chi}_1^0 W^{+*}$	100	$\tilde{\chi}_1^+ \to \tilde{\chi}_1^0 W^{+*} / \tilde{\chi}_2^0 W^{+*}$	75.2/24.7		
$\tilde{\chi}_{2}^{+} \rightarrow \tilde{\chi}_{2}^{0} W^{+} / \tilde{\chi}_{3}^{0} W^{+} / \tilde{\chi}_{1}^{+} Z / \tilde{\chi}_{1}^{+} h_{s}$	40.1/20.4/16.4/11.9	$\tilde{\chi}_{2}^{+} \rightarrow \tilde{\chi}_{1}^{+} Z / \tilde{\chi}_{2}^{0} W^{+} / \tilde{\chi}_{1}^{+} h / \tilde{\chi}_{3}^{0} W^{+} / \tilde{\chi}_{4}^{0} W^{+}$	27.4/22.4/19.4/17.3/6.43		
R value	0.30	R value	0.02		
Signal Region	G05 in CMS-SUS-16-039 [155]	Signal Region	SR2-stop-3high-pt-1 in CMS-SUS-16-048 [157]		

- 3. The consistent interpretation of the scalar anomalies robustly favors the Bino-dominated $\tilde{\chi}_1^0$ as the sole Dark Matter candidate. The measured relic density is achieved through distinct mechanisms in each scenario: **Scenario I** primarily relies on A_s funnel annihilation or coannihilation with \tilde{S} -like $\tilde{\chi}_2^0$ s, and **Scenario II** favors coannihilation with Higgsino-like $\tilde{\chi}_2^0$ s or $\tilde{\chi}_1^{\pm}$ s.
- 4. Constraints from LHC searches for electroweakinos have a negligible impact on the viable parameter space. Full Monte Carlo simulations for benchmark points consistently yield low R-values (< 0.35). This is attributed to the relatively heavy electroweakino masses, which reduce production rates, and the compressed mass spectra,

which lead to detection-challenging soft final states.

5. The necessary non-zero values for the bilinear parameters μ and μ' serve as a direct signature that distinguishes the GNMSSM from the minimal \mathbb{Z}_3 -NMSSM and the MSSM.

In addition to these findings, we provide prospects for several promising search channels targeting a heavy Higgs boson near 650 GeV, presenting posterior probability density functions for key cross-sections and normalized couplings. These projections offer concrete guidance for testing or excluding the GNMSSM parameter space in future analyses. In addition, the benchmark points identified in this work enable reliable extrapolations to the expected sensitivities of the High-Luminosity LHC. Overall, our results highlight the GN-MSSM as a well-motivated extension of the Standard Model that can consistently account for both the observed scalar excesses and a viable dark matter candidate. This motivates continued experimental efforts in forthcoming collider programs and DM detection experiments.

Acknowledgements

This work is supported by the National Natural Science Foundation of China (NNSFC) under Grant No.12447140 and the Natural Science Foundation of Henan Province, China (Grant No. 252300421771, 252300421988)

Appendix

Table A1. Experimental analyses of the electroweakino production processes considered in this study categorizing by the topologies of the SUSY signals.

Scenario	Final State	Name
$\tilde{\chi}_2^0 \tilde{\chi}_1^{\pm} \to W Z \tilde{\chi}_1^0 \tilde{\chi}_1^0$	$n\ell(n\geq 2) + nj(n\geq 0) + \mathbf{E}_{\mathrm{T}}^{\mathrm{miss}}$	$\begin{split} &\text{CMS-SUS-20-001} (137fb^{-1}) \ [158] \\ &\text{ATLAS-2106-01676} (139fb^{-1}) \ [156] \\ &\text{CMS-SUS-17-004} (35.9fb^{-1}) \ [159] \\ &\text{CMS-SUS-16-039} (35.9fb^{-1}) \ [155] \\ &\text{ATLAS-1803-02762} (36.1fb^{-1}) \ [160] \\ &\text{ATLAS-1806-02293} (36.1fb^{-1}) \ [161] \end{split}$
$\tilde{\chi}_2^0 \tilde{\chi}_1^{\pm} \to W h \tilde{\chi}_1^0 \tilde{\chi}_1^0$	$n\ell(n\geq 1) + nb(n\geq 0) + nj(n\geq 0) + \mathbf{E}_{\mathrm{T}}^{\mathrm{miss}}$	$\begin{split} & \text{ATLAS-1909-09226} (139fb^{-1}) [162] \\ & \text{CMS-SUS-17-004} (35.9fb^{-1}) [159] \\ & \text{CMS-SUS-16-039} (35.9fb^{-1}) [155] \\ & \text{ATLAS-1812-09432} (36.1fb^{-1}) [163] \\ & \text{CMS-SUS-16-034} (35.9fb^{-1}) [164] \\ & \text{CMS-SUS-16-045} (35.9fb^{-1}) [165] \end{split}$
$\tilde{\chi}_1^{\mp} \tilde{\chi}_1^{\pm} \to WW \tilde{\chi}_1^0 \tilde{\chi}_1^0$	$2\ell + E_{T}^{miss}$	$\begin{array}{ll} {\rm ATLAS-1908-08215} (139 fb^{-1}) [166] \\ {\rm CMS-SUS-17-010} (35.9 fb^{-1}) [167] \end{array}$
$\begin{array}{l} \tilde{\chi}_2^0 \tilde{\chi}_1^{\pm} \rightarrow ZW \tilde{\chi}_1^0 \tilde{\chi}_1^0 \\ \tilde{\chi}_1^{\pm} \tilde{\chi}_1^{\mp} \rightarrow WW \tilde{\chi}_1^0 \tilde{\chi}_1^0 \end{array}$	$2j(\text{large}) + \mathcal{E}_{\mathcal{T}}^{\text{miss}}$	ATLAS-2108-07586(139 fb^{-1}) [168]
$\begin{array}{l} \tilde{\chi}_2^0 \tilde{\chi}_1^\pm \rightarrow (h/Z) W \tilde{\chi}_1^0 \tilde{\chi}_1^0 \\ \tilde{\chi}_2^0 \tilde{\chi}_3^0 \rightarrow (h/Z) Z \tilde{\chi}_1^0 \tilde{\chi}_1^0 \end{array}$	$j({\rm large}) + b({\rm large}) + {\rm E_T^{miss}}$	${\tt ATLAS-2108-07586(139} fb^{-1})~[168]$
$\begin{array}{l} \tilde{\chi}_2^0 \tilde{\chi}_1^\mp \rightarrow h/ZW \tilde{\chi}_1^0 \tilde{\chi}_1^0, \tilde{\chi}_1^0 \rightarrow \gamma/Z\tilde{G} \\ \tilde{\chi}_1^\pm \tilde{\chi}_1^\mp \rightarrow WW \tilde{\chi}_1^0 \tilde{\chi}_1^0, \tilde{\chi}_1^0 \rightarrow \gamma/Z\tilde{G} \end{array}$	$2\gamma + n\ell(n \ge 0) + nb(n \ge 0) + nj(n \ge 0) + \mathcal{E}_{\mathcal{T}}^{\text{miss}}$	ATLAS-1802-03158(36.1 fb^{-1}) [169]
$\begin{array}{l} \tilde{\chi}_{2}^{0}\tilde{\chi}_{1}^{\pm} \to ZW\tilde{\chi}_{1}^{0}\tilde{\chi}_{1}^{0},\tilde{\chi}_{1}^{0} \to h/Z\tilde{G} \\ \tilde{\chi}_{1}^{\pm}\tilde{\chi}_{1}^{\mp} \to WW\tilde{\chi}_{1}^{0}\tilde{\chi}_{1}^{0},\tilde{\chi}_{1}^{0} \to h/Z\tilde{G} \\ \tilde{\chi}_{2}^{0}\tilde{\chi}_{1}^{0} \to Z\tilde{\chi}_{1}^{0}\tilde{\chi}_{1}^{0},\tilde{\chi}_{1}^{0} \to h/Z\tilde{G} \\ \tilde{\chi}_{1}^{\mp}\tilde{\chi}_{1}^{0} \to W\tilde{\chi}_{1}^{0}\tilde{\chi}_{1}^{0},\tilde{\chi}_{1}^{0} \to h/Z\tilde{G} \end{array}$	$n\ell(n \geq 4) + \mathrm{E_T^{miss}}$	${\tt ATLAS-2103-11684(139} fb^{-1}) \ [170]$
$\tilde{\chi}_{i}^{0,\pm}\tilde{\chi}_{j}^{0,\mp}\rightarrow\tilde{\chi}_{1}^{0}\tilde{\chi}_{1}^{0}+\chi_{soft}\rightarrow ZZ/H\tilde{G}\tilde{G}$	$n\ell(n\geq 2) + nb(n\geq 0) + nj(n\geq 0) + \mathbf{E}_{\mathrm{T}}^{\mathrm{miss}}$	$\begin{array}{l} {\rm CMS-SUS-16-039} (35.9 fb^{-1}) [155] \\ {\rm CMS-SUS-17-004} (35.9 fb^{-1}) [159] \\ {\rm CMS-SUS-20-001} (137 fb^{-1}) [158] \end{array}$
$\tilde{\chi}_{i}^{0,\pm}\tilde{\chi}_{j}^{0,\mp}\rightarrow\tilde{\chi}_{1}^{0}\tilde{\chi}_{1}^{0}+\chi_{soft}\rightarrow HH\tilde{G}\tilde{G}$	$n\ell(n\geq 2) + nb(n\geq 0) + nj(n\geq 0) + \mathbf{E}_{\mathrm{T}}^{\mathrm{miss}}$	$\begin{array}{c} \text{CMS-SUS-16-039} (35.9 fb^{-1}) [155] \\ \text{CMS-SUS-17-004} (35.9 fb^{-1}) [159] \end{array}$
$\tilde{\chi}^0_2 \tilde{\chi}^\pm_1 \to W^* Z^* \tilde{\chi}^0_1 \tilde{\chi}^0_1$	$3\ell + E_{\rm T}^{\rm miss}$	ATLAS-2106-01676(139 fb^{-1}) [156]
$\tilde{\chi}_2^0 \tilde{\chi}_1^\pm \to Z^* W^* \tilde{\chi}_1^0 \tilde{\chi}_1^0$	$2\ell + nj(n \ge 0) + E_{\mathrm{T}}^{\mathrm{miss}}$	$\begin{split} & \text{ATLAS-1911-12606} (139 fb^{-1}) \ [171] \\ & \text{ATLAS-1712-08119} (36.1 fb^{-1}) \ [172] \\ & \text{CMS-SUS-16-048} (35.9 fb^{-1}) \ [157] \end{split}$
$\tilde{\chi}_{1}^{0}\tilde{\chi}_{1}^{\pm} + \tilde{\chi}_{1}^{\pm}\tilde{\chi}_{1}^{\mp} + \tilde{\chi}_{1}^{\pm}\tilde{\chi}_{1}^{0}$	$2\ell + nj(n \ge 0) + \mathcal{E}_{\mathcal{T}}^{\text{miss}}$	$\begin{split} & \text{ATLAS-1911-12606} (139 fb^{-1}) [171] \\ & \text{ATLAS-1712-08119} (36.1 fb^{-1}) [172] \\ & \text{CMS-SUS-16-048} (35.9 fb^{-1}) [157] \end{split}$

References

[1] LEP WORKING GROUP FOR HIGGS BOSON SEARCHES, ALEPH, DELPHI, L3, OPAL collaboration, R. Barate et al., Search for the standard model Higgs boson at LEP, Phys. Lett. B 565 (2003) 61 [hep-ex/0306033].

- [2] A. Azatov, R. Contino and J. Galloway, Model-Independent Bounds on a Light Higgs, JHEP 04 (2012) 127 [1202.3415].
- [3] J. Cao, X. Guo, Y. He, P. Wu and Y. Zhang, Diphoton signal of the light Higgs boson in natural NMSSM, Phys. Rev. D 95 (2017) 116001 [1612.08522].
- [4] CMS collaboration, "Search for new resonances in the diphoton final state in the mass range between 80 and 115 GeV in pp collisions at $\sqrt{s} = 8$ TeV." CMS-PAS-HIG-14-037, 2015.
- [5] CMS collaboration, "Search for a standard model-like Higgs boson in the mass range between 70 and 110 GeV in the diphoton final state in proton-proton collisions at $\sqrt{s} = 13$ TeV." CMS-PAS-HIG-20-002, 2023.
- [6] C. Arcangeletti. on behalf of ATLAS collaboration, LHC Seminar https://indico.cern.ch/event/1281604/attachments/2660420/4608571/ LHCSeminarArcangeletti_final.pdf, 7th of June, 2023.
- [7] T. Biekötter, S. Heinemeyer and G. Weiglein, 95.4 GeV diphoton excess at ATLAS and CMS, Phys. Rev. D 109 (2024) 035005 [2306.03889].
- [8] CMS collaboration, A. Tumasyan et al., Searches for additional Higgs bosons and for vector leptoquarks in $\tau\tau$ final states in proton-proton collisions at $\sqrt{s}=13$ TeV, JHEP **07** (2023) 073 [2208.02717].
- [9] G. Coloretti, A. Crivellin, S. Bhattacharya and B. Mellado, Searching for low-mass resonances decaying into W bosons, Phys. Rev. D 108 (2023) 035026 [2302.07276].
- [10] CMS collaboration, A. Tumasyan et al., Search for a new resonance decaying into two spin-0 bosons in a final state with two photons and two bottom quarks in proton-proton collisions at $\sqrt{s} = 13$ TeV, JHEP **05** (2024) 316 [2310.01643].
- [11] U. Ellwanger and C. Hugonie, Additional Higgs Bosons near 95 and 650 GeV in the NMSSM, Eur. Phys. J. C 83 (2023) 1138 [2309.07838].
- [12] CMS collaboration, A. Tumasyan et al., Search for a heavy Higgs boson decaying into two lighter Higgs bosons in the $\tau\tau bb$ final state at 13 TeV, JHEP 11 (2021) 057 [2106.10361].
- [13] S. Ashanujjaman, S. Banik, G. Coloretti, A. Crivellin, B. Mellado and A.-T. Mulaudzi, SU(2)L triplet scalar as the origin of the 95 GeV excess?, Phys. Rev. D 108 (2023) L091704 [2306.15722].
- [14] J. A. Aguilar-Saavedra and F. R. Joaquim, Multiphoton signals of a (96 GeV?) stealth boson, Eur. Phys. J. C 80 (2020) 403 [2002.07697].
- [15] A. Kundu, S. Maharana and P. Mondal, A 96 GeV scalar tagged to dark matter models, Nucl. Phys. B 955 (2020) 115057 [1907.12808].
- [16] P. J. Fox and N. Weiner, Light Signals from a Lighter Higgs, JHEP 08 (2018) 025 [1710.07649].
- [17] A. Belyaev, R. Benbrik, M. Boukidi, M. Chakraborti, S. Moretti and S. Semlali, Explanation of the hints for a 95 GeV Higgs boson within a 2-Higgs Doublet Model, JHEP 05 (2024) 209 [2306.09029].
- [18] D. Azevedo, T. Biekötter and P. M. Ferreira, 2HDM interpretations of the CMS diphoton excess at 95 GeV, JHEP 11 (2023) 017 [2305.19716].

- [19] R. Benbrik, M. Boukidi and B. Manaut, Interpreting the W-mass and muon $(g_{\mu} 2)$ anomalies within a 2-Higgs doublet model, Nucl. Phys. B 1005 (2024) 116593 [2204.11755].
- [20] R. Benbrik, M. Boukidi, S. Moretti and S. Semlali, Explaining the 96 GeV Di-photon anomaly in a generic 2HDM Type-III, Phys. Lett. B 832 (2022) 137245 [2204.07470].
- [21] U. Haisch and A. Malinauskas, Let there be light from a second light Higgs doublet, JHEP 03 (2018) 135 [1712.06599].
- [22] T. Biekötter, M. Chakraborti and S. Heinemeyer, An N2HDM Solution for the possible 96 GeV Excess, PoS CORFU2018 (2019) 015 [1905.03280].
- [23] T. Biekötter, M. Chakraborti and S. Heinemeyer, A 96 GeV Higgs boson in the N2HDM, Eur. Phys. J. C 80 (2020) 2 [1903.11661].
- [24] T. Biekötter, M. Chakraborti and S. Heinemeyer, The "96 GeV excess" at the LHC, Int. J. Mod. Phys. A 36 (2021) 2142018 [2003.05422].
- [25] T. Biekötter and M. O. Olea-Romacho, Reconciling Higgs physics and pseudo-Nambu-Goldstone dark matter in the S2HDM using a genetic algorithm, JHEP 10 (2021) 215 [2108.10864].
- [26] S. Heinemeyer, C. Li, F. Lika, G. Moortgat-Pick and S. Paasch, *Phenomenology of a 96 GeV Higgs boson in the 2HDM with an additional singlet*, *Phys. Rev. D* **106** (2022) 075003 [2112.11958].
- [27] T. Biekötter, S. Heinemeyer and G. Weiglein, Mounting evidence for a 95 GeV Higgs boson, JHEP 08 (2022) 201 [2203.13180].
- [28] C. Li, *Phenomenology of extended Two-Higgs-Doublets models*, Ph.D. thesis, Hamburg U., 2023. 10.3204/PUBDB-2023-03151.
- [29] T. Biekötter, S. Heinemeyer and G. Weiglein, The CMS di-photon excess at 95 GeV in view of the LHC Run 2 results, Phys. Lett. B 846 (2023) 138217 [2303.12018].
- [30] J. A. Aguilar-Saavedra, H. B. Câmara, F. R. Joaquim and J. F. Seabra, Confronting the 95 GeV excesses within the UN2HDM, 2307.03768.
- [31] S. Banik, A. Crivellin, S. Iguro and T. Kitahara, Asymmetric di-Higgs signals of the next-to-minimal 2HDM with a U(1) symmetry, Phys. Rev. D 108 (2023) 075011 [2303.11351].
- [32] J. Dutta, J. Lahiri, C. Li, G. Moortgat-Pick, S. F. Tabira and J. A. Ziegler, Dark matter phenomenology in 2HDMS in light of the 95 GeV excess, Eur. Phys. J. C 84 (2024) 926 [2308.05653].
- [33] D. Sachdeva and S. Sadhukhan, Discussing 125 GeV and 95 GeV excess in light radion model, Phys. Rev. D 101 (2020) 055045 [1908.01668].
- [34] R. Vega, R. Vega-Morales and K. Xie, Light (and darkness) from a light hidden Higgs, JHEP 06 (2018) 137 [1805.01970].
- [35] D. Borah, S. Mahapatra, P. K. Paul and N. Sahu, Scotogenic $U(1)L\mu$ - $L\tau$ origin of $(g-2)\mu$, W-mass anomaly and 95 GeV excess, Phys. Rev. D 109 (2024) 055021 [2310.11953].
- [36] G. Arcadi, G. Busoni, D. Cabo-Almeida and N. Krishnan, Is there a scalar or pseudoscalar at 95 GeV?, Phys. Rev. D 110 (2024) 115028 [2311.14486].
- [37] A. Ahriche, 95 GeV excess in the Georgi-Machacek model: Single or twin peak resonance, Phys. Rev. D 110 (2024) 035010 [2312.10484].

- [38] T.-K. Chen, C.-W. Chiang, S. Heinemeyer and G. Weiglein, 95 GeV Higgs boson in the Georgi-Machacek model, Phys. Rev. D 109 (2024) 075043 [2312.13239].
- [39] P. S. B. Dev, R. N. Mohapatra and Y. Zhang, Explanation of the 95 GeV $\gamma\gamma$ and bb excesses in the minimal left-right symmetric model, Phys. Lett. B 849 (2024) 138481 [2312.17733].
- [40] K. Wang and J. Zhu, 95 GeV light Higgs in the top-pair-associated diphoton channel at the LHC in the minimal dilaton model*, Chin. Phys. C 48 (2024) 073105 [2402.11232].
- [41] J.-W. Fan, J.-Q. Tao, Y.-Q. Shen, G.-M. Chen, H.-S. Chen, S. Gascon-Shotkin et al., Study of diphoton decays of the lightest scalar Higgs boson in the Next-to-Minimal Supersymmetric Standard Model, Chin. Phys. C 38 (2014) 073101 [1309.6394].
- [42] T. Biekötter, S. Heinemeyer and C. Muñoz, Precise prediction for the Higgs-boson masses in the μν SSM, Eur. Phys. J. C 78 (2018) 504 [1712.07475].
- [43] C. Beskidt, W. de Boer and D. I. Kazakov, Can we discover a light singlet-like NMSSM Higgs boson at the LHC?, Phys. Lett. B 782 (2018) 69 [1712.02531].
- [44] S. Heinemeyer and T. Stefaniak, A Higgs Boson at 96 GeV?!, PoS CHARGED2018 (2019) 016 [1812.05864].
- [45] S. Heinemeyer, A Higgs boson below 125 GeV?!, Int. J. Mod. Phys. A 33 (2018) 1844006.
- [46] K. Wang, F. Wang, J. Zhu and Q. Jie, The semi-constrained NMSSM in light of muon g-2, LHC, and dark matter constraints, Chin. Phys. C 42 (2018) 103109 [1811.04435].
- [47] F. Domingo, S. Heinemeyer, S. Paßehr and G. Weiglein, Decays of the neutral Higgs bosons into SM fermions and gauge bosons in the CP-violating NMSSM, Eur. Phys. J. C 78 (2018) 942 [1807.06322].
- [48] J. Cao, X. Jia, Y. Yue, H. Zhou and P. Zhu, 96 GeV diphoton excess in seesaw extensions of the natural NMSSM, Phys. Rev. D 101 (2020) 055008 [1908.07206].
- [49] T. Biekötter, S. Heinemeyer and C. Muñoz, Precise prediction for the Higgs-Boson masses in the μνSSM with three right-handed neutrino superfields, Eur. Phys. J. C 79 (2019) 667 [1906.06173].
- [50] K. Choi, S. H. Im, K. S. Jeong and C. B. Park, Light Higgs bosons in the general NMSSM, Eur. Phys. J. C 79 (2019) 956 [1906.03389].
- [51] A. A. Abdelalim, B. Das, S. Khalil and S. Moretti, Di-photon decay of a light Higgs state in the BLSSM, Nucl. Phys. B 985 (2022) 116013 [2012.04952].
- [52] W. G. Hollik, C. Li, G. Moortgat-Pick and S. Paasch, Phenomenology of a Supersymmetric Model Inspired by Inflation, Eur. Phys. J. C 81 (2021) 141 [2004.14852].
- [53] T. Biekötter, A. Grohsjean, S. Heinemeyer, C. Schwanenberger and G. Weiglein, Possible indications for new Higgs bosons in the reach of the LHC: N2HDM and NMSSM interpretations, Eur. Phys. J. C 82 (2022) 178 [2109.01128].
- [54] W. Li, H. Qiao and J. Zhu, Light Higgs boson in the NMSSM confronted with the CMS di-photon and di-tau excesses*, Chin. Phys. C 47 (2023) 123102 [2212.11739].
- [55] J. Cao, X. Jia, J. Lian and L. Meng, 95 GeV diphoton and bb excesses in the general next-to-minimal supersymmetric standard model, Phys. Rev. D 109 (2024) 075001 [2310.08436].

- [56] A. Ahriche, M. L. Bellilet, M. O. Khojali, M. Kumar and A.-T. Mulaudzi, Scale invariant scotogenic model: CDF-II W-boson mass and the 95 GeV excesses, Phys. Rev. D 110 (2024) 015025 [2311.08297].
- [57] U. Ellwanger and C. Hugonie, Nmssm with correct relic density and an additional 95 GeV Higgs boson, Eur. Phys. J. C 84 (2024) 526 [2403.16884].
- [58] J. Lian, 95 GeV excesses in the Z3-symmetric next-to-minimal supersymmetric standard model, Phys. Rev. D 110 (2024) 115018 [2406.10969].
- [59] J. Cao, X. Jia and J. Lian, Unified interpretation of the muon g-2 anomaly, the 95 GeV diphoton, and bb excesses in the general next-to-minimal supersymmetric standard model, Phys. Rev. D 110 (2024) 115039 [2402.15847].
- [60] C.-X. Liu, Y. Zhou, X.-Y. Zheng, J. Ma, T.-F. Feng and H.-B. Zhang, 95 GeV excess in a CP-violating μ-from-ν SSM, Phys. Rev. D 109 (2024) 056001 [2402.00727].
- [61] U. Ellwanger, C. Hugonie, S. F. King and S. Moretti, NMSSM explanation for excesses in the search for neutralinos and charginos and a 95 GeV Higgs boson, Eur. Phys. J. C 84 (2024) 788 [2404.19338].
- [62] H. Xu, Y. Wang, X.-F. Han and L. Wang, 95 GeV Higgs boson and nano-Hertz gravitational waves from domain walls in the N2HDM, 2505.03592.
- [63] G. Abbas, V. Singh and N. Singh, Dark-technicolour at colliders, 2504.21593.
- [64] Z. Li, N. Liu and B. Zhu, Interplay of 95 GeV Diphoton Excess and Dark Matter in Supersymmetric Triplet Model, 2504.21273.
- [65] X. Du, H. Liu and Q. Chang, Interpretation of 95 GeV excess within the Georgi-Machacek model in light of positive definiteness constraints, Phys. Rev. D 112 (2025) 015019 [2502.06444].
- [66] S. Gao, S.-M. Zhao, S. Di, X.-X. Dong and T.-F. Feng, A 95 GeV Higgs boson in the U(1)XSSM, Nucl. Phys. B 1018 (2025) 117026 [2411.13261].
- [67] J. Gao, X.-F. Han, J. Ma, L. Wang and H. Xu, 95 GeV Higgs boson and spontaneous CP-violation at the finite temperature, Phys. Rev. D 110 (2024) 115045 [2408.03705].
- [68] R. Benbrik, M. Boukidi, K. Kahime, S. Moretti, L. Rahili and B. Taki, Exploring potential Higgs resonances at 650 GeV and 95 GeV in the 2HDM Type III, Phys. Lett. B 868 (2025) 139688 [2505.07811].
- [69] U. Ellwanger, C. Hugonie and A. M. Teixeira, *The Next-to-Minimal Supersymmetric Standard Model*, *Phys. Rept.* **496** (2010) 1 [0910.1785].
- [70] M. Maniatis, The Next-to-Minimal Supersymmetric extension of the Standard Model reviewed, Int. J. Mod. Phys. A 25 (2010) 3505 [0906.0777].
- [71] A. Hammad, R. Ramos, A. Chakraborty, P. Ko and S. Moretti, Explaining Data Anomalies over the NMSSM Parameter Space with Deep Learning Techniques, 2508.13912.
- [72] U. Ellwanger and A. M. Teixeira, NMSSM with a singlino LSP: possible challenges for searches for supersymmetry at the LHC, JHEP 10 (2014) 113 [1406.7221].
- [73] J. Cao, D. Li, J. Lian, Y. Yue and H. Zhou, Singlino-dominated dark matter in general NMSSM, JHEP 06 (2021) 176 [2102.05317].

- [74] J. Cao, L. Meng, Y. Yue, H. Zhou and P. Zhu, Suppressing the scattering of WIMP dark matter and nucleons in supersymmetric theories, Phys. Rev. D 101 (2020) 075003 [1910.14317].
- [75] U. Ellwanger, A Higgs boson near 125 GeV with enhanced di-photon signal in the NMSSM, JHEP 03 (2012) 044 [1112.3548].
- [76] M. Badziak, M. Olechowski and S. Pokorski, New Regions in the NMSSM with a 125 GeV Higgs, JHEP 06 (2013) 043 [1304.5437].
- [77] J.-J. Cao, Z.-X. Heng, J. M. Yang, Y.-M. Zhang and J.-Y. Zhu, A SM-like Higgs near 125 GeV in low energy SUSY: a comparative study for MSSM and NMSSM, JHEP 03 (2012) 086 [1202.5821].
- [78] U. Ellwanger, Nonrenormalizable interactions from supergravity, quantum corrections and effective low-energy theories, Phys. Lett. B 133 (1983) 187.
- [79] S. A. Abel, Destabilizing divergences in the NMSSM, Nucl. Phys. B 480 (1996) 55 [hep-ph/9609323].
- [80] C. F. Kolda, S. Pokorski and N. Polonsky, Stabilized singlets in supergravity as a source of the mu - parameter, Phys. Rev. Lett. 80 (1998) 5263 [hep-ph/9803310].
- [81] C. Panagiotakopoulos and K. Tamvakis, Stabilized NMSSM without domain walls, Phys. Lett. B 446 (1999) 224 [hep-ph/9809475].
- [82] G. G. Ross and K. Schmidt-Hoberg, The Fine-Tuning of the Generalised NMSSM, Nucl. Phys. B 862 (2012) 710 [1108.1284].
- [83] H. M. Lee, S. Raby, M. Ratz, G. G. Ross, R. Schieren, K. Schmidt-Hoberg et al., A unique \mathbb{Z}_4^R symmetry for the MSSM, Phys. Lett. B **694** (2011) 491 [1009.0905].
- [84] H. M. Lee, S. Raby, M. Ratz, G. G. Ross, R. Schieren, K. Schmidt-Hoberg et al., Discrete R symmetries for the MSSM and its singlet extensions, Nucl. Phys. B 850 (2011) 1 [1102.3595].
- [85] G. G. Ross, K. Schmidt-Hoberg and F. Staub, The Generalised NMSSM at One Loop: Fine Tuning and Phenomenology, JHEP 08 (2012) 074 [1205.1509].
- [86] D. J. Miller, R. Nevzorov and P. M. Zerwas, *The Higgs sector of the next-to-minimal supersymmetric standard model*, *Nucl. Phys. B* **681** (2004) 3 [hep-ph/0304049].
- [87] M. Carena, H. E. Haber, I. Low, N. R. Shah and C. E. M. Wagner, Alignment limit of the NMSSM Higgs sector, Phys. Rev. D 93 (2016) 035013 [1510.09137].
- [88] ATLAS collaboration, G. Aad et al., Search for heavy Higgs bosons decaying into two tau leptons with the ATLAS detector using pp collisions at $\sqrt{s} = 13$ TeV, Phys. Rev. Lett. 125 (2020) 051801 [2002.12223].
- [89] ATLAS collaboration, A detailed map of Higgs boson interactions by the ATLAS experiment ten years after the discovery, Nature 607 (2022) 52 [2207.00092].
- [90] CMS collaboration, A. Tumasyan et al., A portrait of the Higgs boson by the CMS experiment ten years after the discovery, Nature 607 (2022) 60 [2207.00043].
- [91] S. Baum, M. Carena, N. R. Shah and C. E. M. Wagner, Higgs portals for thermal Dark Matter. EFT perspectives and the NMSSM, JHEP 04 (2018) 069 [1712.09873].
- [92] L. Meng, J. Cao, F. Li and S. Yang, Dark Matter physics in general NMSSM, JHEP 08 (2024) 212 [2405.07036].

- [93] F. Staub, SARAH, 0806.0538.
- [94] F. Staub, SARAH 3.2: Dirac Gauginos, UFO output, and more, Comput. Phys. Commun. 184 (2013) 1792 [1207.0906].
- [95] F. Staub, SARAH 4: A tool for (not only SUSY) model builders, Comput. Phys. Commun. 185 (2014) 1773 [1309.7223].
- [96] F. Staub, Exploring new models in all detail with SARAH, Adv. High Energy Phys. 2015 (2015) 840780 [1503.04200].
- [97] W. Porod, SPheno, a program for calculating supersymmetric spectra, SUSY particle decays and SUSY particle production at e+ e- colliders, Comput. Phys. Commun. 153 (2003) 275 [hep-ph/0301101].
- [98] W. Porod and F. Staub, SPheno 3.1: Extensions including flavour, CP-phases and models beyond the MSSM, Comput. Phys. Commun. 183 (2012) 2458 [1104.1573].
- [99] W. Porod, F. Staub and A. Vicente, A Flavor Kit for BSM models, Eur. Phys. J. C 74 (2014) 2992 [1405.1434].
- [100] G. Belanger, F. Boudjema, A. Pukhov and A. Semenov, MicrOMEGAs: A Program for calculating the relic density in the MSSM, Comput. Phys. Commun. 149 (2002) 103 [hep-ph/0112278].
- [101] G. Bélanger, F. Boudjema, A. Pukhov and A. Semenov, micrOMEGAs: Version 1.3, Comput. Phys. Commun. 174 (2006) 577 [hep-ph/0405253].
- [102] G. Bélanger, F. Boudjema, C. Hugonie, A. Pukhov and A. Semenov, Relic density of dark matter in the NMSSM, JCAP 09 (2005) 001 [hep-ph/0505142].
- [103] G. Bélanger, F. Boudjema, A. Pukhov and A. Semenov, MicrOMEGAs 2.0: A Program to calculate the relic density of dark matter in a generic model, Comput. Phys. Commun. 176 (2007) 367 [hep-ph/0607059].
- [104] G. Bélanger, F. Boudjema, S. Kraml, A. Pukhov and A. Semenov, Relic density of neutralino dark matter in the MSSM with CP violation, Phys. Rev. D 73 (2006) 115007 [hep-ph/0604150].
- [105] G. Bélanger, F. Boudjema, A. Pukhov and A. Semenov, Dark matter direct detection rate in a generic model with micrOMEGAs 2.2, Comput. Phys. Commun. 180 (2009) 747 [0803.2360].
- [106] G. Belanger, F. Boudjema, A. Pukhov and A. Semenov, micrOMEGAs: A Tool for dark matter studies, Nuovo Cim. C 033N2 (2010) 111 [1005.4133].
- [107] Bélanger, G. and Boudjema, F. and Pukhov, A. and Semenov, A., micrOMEGAs_3: A program for calculating dark matter observables, Comput. Phys. Commun. 185 (2014) 960 [1305.0237].
- [108] D. Barducci, G. Belanger, J. Bernon, F. Boudjema, J. Da Silva, S. Kraml et al., Collider limits on new physics within micrOMEGAs_4.3, Comput. Phys. Commun. 222 (2018) 327 [1606.03834].
- [109] G. Bélanger, F. Boudjema, A. Goudelis, A. Pukhov and B. Zaldivar, micrOMEGAs5.0: Freeze-in, Comput. Phys. Commun. 231 (2018) 173 [1801.03509].
- [110] A. Fowlie and M. H. Bardsley, Superplot: a graphical interface for plotting and analysing MultiNest output, Eur. Phys. J. Plus 131 (2016) 391 [1603.00555].

- [111] S. F. King and P. L. White, Resolving the constrained minimal and next-to-minimal supersymmetric standard models, Phys. Rev. D 52 (1995) 4183 [hep-ph/9505326].
- [112] M. Masip, R. Munoz-Tapia and A. Pomarol, Limits on the mass of the lightest Higgs in supersymmetric models, Phys. Rev. D 57 (1998) R5340 [hep-ph/9801437].
- [113] F. Feroz, M. P. Hobson and M. Bridges, MultiNest: an efficient and robust Bayesian inference tool for cosmology and particle physics, Mon. Not. Roy. Astron. Soc. 398 (2009) 1601 [0809.3437].
- [114] F. Feroz, M. P. Hobson, E. Cameron and A. N. Pettitt, Importance Nested Sampling and the MultiNest Algorithm, Open J. Astrophys. 2 (2019) 10 [1306.2144].
- [115] P. Bechtle, S. Heinemeyer, O. Stål, T. Stefaniak and G. Weiglein, HiggsSignals: Confronting arbitrary Higgs sectors with measurements at the Tevatron and the LHC, Eur. Phys. J. C 74 (2014) 2711 [1305.1933].
- [116] O. Stål and T. Stefaniak, Constraining extended Higgs sectors with HiggsSignals, PoS EPS-HEP2013 (2013) 314 [1310.4039].
- [117] P. Bechtle, S. Heinemeyer, O. Stål, T. Stefaniak and G. Weiglein, Probing the Standard Model with Higgs signal rates from the Tevatron, the LHC and a future ILC, JHEP 11 (2014) 039 [1403.1582].
- [118] P. Bechtle, S. Heinemeyer, T. Klingl, T. Stefaniak, G. Weiglein and J. Wittbrodt, HiggsSignals-2: Probing new physics with precision Higgs measurements in the LHC 13 TeV era, Eur. Phys. J. C 81 (2021) 145 [2012.09197].
- [119] M. Mühlleitner, M. O. P. Sampaio, R. Santos and J. Wittbrodt, ScannerS: parameter scans in extended scalar sectors, Eur. Phys. J. C 82 (2022) 198 [2007.02985].
- [120] H. Bahl, T. Biekötter, S. Heinemeyer, C. Li, S. Paasch, G. Weiglein et al., *HiggsTools: BSM scalar phenomenology with new versions of HiggsBounds and HiggsSignals, Comput. Phys. Commun.* **291** (2023) 108803 [2210.09332].
- [121] P. Bechtle, O. Brein, S. Heinemeyer, G. Weiglein and K. E. Williams, HiggsBounds: Confronting Arbitrary Higgs Sectors with Exclusion Bounds from LEP and the Tevatron, Comput. Phys. Commun. 181 (2010) 138 [0811.4169].
- [122] P. Bechtle, O. Brein, S. Heinemeyer, G. Weiglein and K. E. Williams, HiggsBounds 2.0.0: Confronting Neutral and Charged Higgs Sector Predictions with Exclusion Bounds from LEP and the Tevatron, Comput. Phys. Commun. 182 (2011) 2605 [1102.1898].
- [123] P. Bechtle, O. Brein, S. Heinemeyer, O. Stal, T. Stefaniak, G. Weiglein et al., Recent Developments in HiggsBounds and a Preview of HiggsSignals, PoS CHARGED2012 (2012) 024 [1301.2345].
- [124] P. Bechtle, O. Brein, S. Heinemeyer, O. Stål, T. Stefaniak, G. Weiglein et al., HiggsBounds – 4: Improved Tests of Extended Higgs Sectors against Exclusion Bounds from LEP, the Tevatron and the LHC, Eur. Phys. J. C 74 (2014) 2693 [1311.0055].
- [125] P. Bechtle, D. Dercks, S. Heinemeyer, T. Klingl, T. Stefaniak, G. Weiglein et al., HiggsBounds-5: Testing Higgs Sectors in the LHC 13 TeV Era, Eur. Phys. J. C 80 (2020) 1211 [2006.06007].
- [126] Planck collaboration, N. Aghanim et al., *Planck 2018 results. VI. Cosmological parameters*, *Astron. Astrophys.* **641** (2020) A6 [1807.06209].

- [127] LZ collaboration, J. Aalbers et al., Dark Matter Search Results from 4.2 Tonne-Years of Exposure of the LUX-ZEPLIN (LZ) Experiment, Phys. Rev. Lett. 135 (2025) 011802 [2410.17036].
- [128] S. Haselschwardt, "New dark matter search results from the lux-zeplin (lz) experiment." https://indico.uchicago.edu/event/427/contributions/1325/attachments/359/548/lz_results_tevpa.pdf, 2024.
- [129] FERMI-LAT collaboration, M. Ackermann et al., Searching for Dark Matter Annihilation from Milky Way Dwarf Spheroidal Galaxies with Six Years of Fermi Large Area Telescope Data, Phys. Rev. Lett. 115 (2015) 231301 [1503.02641].
- [130] Particle Data Group collaboration, S. Navas et al., Review of particle physics, Phys. Rev. D 110 (2024) 030001.
- [131] W. G. Hollik, G. Weiglein and J. Wittbrodt, Impact of Vacuum Stability Constraints on the Phenomenology of Supersymmetric Models, JHEP 03 (2019) 109 [1812.04644].
- [132] B. O'Leary and J. E. Camargo-Molina, "VevaciousPlusPlus." https://github.com/JoseEliel/VevaciousPlusPlus, 2014.
- [133] J. E. Camargo-Molina, B. O'Leary, W. Porod and F. Staub, Vevacious: A Tool For Finding The Global Minima Of One-Loop Effective Potentials With Many Scalars, Eur. Phys. J. C 73 (2013) 2588 [1307.1477].
- [134] ATLAS collaboration, G. Aad et al., A statistical combination of ATLAS Run 2 searches for charginos and neutralinos at the LHC, 2402.08347.
- [135] C. K. Khosa, S. Kraml, A. Lessa, P. Neuhuber and W. Waltenberger, *SModelS database update v1.2.3*, 2005.00555.
- [136] J. Alwall, M. Herquet, F. Maltoni, O. Mattelaer and T. Stelzer, MadGraph 5: Going Beyond, JHEP 06 (2011) 128 [1106.0522].
- [137] E. Conte, B. Fuks and G. Serret, MadAnalysis 5, A User-Friendly Framework for Collider Phenomenology, Comput. Phys. Commun. 184 (2013) 222 [1206.1599].
- [138] W. Beenakker, R. Hopker and M. Spira, *PROSPINO: A Program for the production of supersymmetric particles in next-to-leading order QCD*, hep-ph/9611232.
- [139] T. Sjöstrand, S. Ask, J. R. Christiansen, R. Corke, N. Desai, P. Ilten et al., An introduction to PYTHIA 8.2, Comput. Phys. Commun. 191 (2015) 159 [1410.3012].
- [140] DELPHES 3 collaboration, J. de Favereau, C. Delaere, P. Demin, A. Giammanco, V. Lemaître, A. Mertens et al., DELPHES 3, A modular framework for fast simulation of a generic collider experiment, JHEP 02 (2014) 057 [1307.6346].
- [141] M. Drees, H. Dreiner, D. Schmeier, J. Tattersall and J. S. Kim, CheckMATE: Confronting your Favourite New Physics Model with LHC Data, Comput. Phys. Commun. 187 (2015) 227 [1312.2591].
- [142] D. Dercks, N. Desai, J. S. Kim, K. Rolbiecki, J. Tattersall and T. Weber, CheckMATE 2: From the model to the limit, Comput. Phys. Commun. 221 (2017) 383 [1611.09856].
- [143] J. S. Kim, D. Schmeier, J. Tattersall and K. Rolbiecki, A framework to create customised LHC analyses within CheckMATE, Comput. Phys. Commun. 196 (2015) 535 [1503.01123].
- [144] J. Cao, J. Lian, Y. Pan, D. Zhang and P. Zhu, Improved $(g-2)_{\mu}$ measurement and singlino dark matter in μ -term extended \mathbb{Z}_3 -NMSSM, JHEP **09** (2021) 175 [2104.03284].

- [145] F. Feroz, M. P. Hobson, E. Cameron and A. N. Pettitt, *Importance Nested Sampling and the MultiNest Algorithm*, *Open J. Astrophys.* **2** (2019) 10 [1306.2144].
- [146] F. Feroz, M. P. Hobson and M. Bridges, MultiNest: an efficient and robust Bayesian inference tool for cosmology and particle physics, Mon. Not. Roy. Astron. Soc. 398 (2009) 1601 [0809.3437].
- [147] F. Feroz and M. P. Hobson, Multimodal nested sampling: an efficient and robust alternative to MCMC methods for astronomical data analysis, Mon. Not. Roy. Astron. Soc. 384 (2008) 449 [0704.3704].
- [148] J. Skilling, Nested sampling for general Bayesian computation, Bayesian Analysis 1 (2006) 833.
- [149] CMS collaboration, A. M. Sirunyan et al., Search for a heavy pseudoscalar boson decaying to a Z and a Higgs boson at $\sqrt{s} = 13$ TeV, Eur. Phys. J. C 79 (2019) 564 [1903.00941].
- [150] ATLAS collaboration, G. Aad et al., Search for heavy resonances decaying into a Z or W boson and a Higgs boson in final states with leptons and b-jets in 139 fb⁻¹ of pp collisions at $\sqrt{s} = 13$ TeV with the ATLAS detector, JHEP 06 (2023) 016 [2207.00230].
- [151] CMS collaboration, A. M. Sirunyan et al., Search for new neutral Higgs bosons through the $H \rightarrow ZA \rightarrow \ell^+\ell^-$ bb process in pp collisions at $\sqrt{s} = 13$ TeV, JHEP **03** (2020) 055 [1911.03781].
- [152] CMS collaboration, A. M. Sirunyan et al., Search for heavy Higgs bosons decaying to a top quark pair in proton-proton collisions at $\sqrt{s} = 13$ TeV, JHEP **04** (2020) 171 [1908.01115].
- [153] LZ collaboration, D. S. Akerib et al., Projected WIMP sensitivity of the LUX-ZEPLIN dark matter experiment, Phys. Rev. D 101 (2020) 052002 [1802.06039].
- [154] J. Billard, L. Strigari and E. Figueroa-Feliciano, Implication of neutrino backgrounds on the reach of next generation dark matter direct detection experiments, Phys. Rev. D 89 (2014) 023524 [1307.5458].
- [155] CMS collaboration, A. M. Sirunyan et al., Search for electroweak production of charginos and neutralinos in multilepton final states in proton-proton collisions at $\sqrt{s} = 13$ TeV, JHEP 03 (2018) 166 [1709.05406].
- [156] ATLAS collaboration, G. Aad et al., Search for chargino-neutralino pair production in final states with three leptons and missing transverse momentum in $\sqrt{s} = 13$ TeV pp collisions with the ATLAS detector, Eur. Phys. J. C 81 (2021) 1118 [2106.01676].
- [157] CMS collaboration, A. M. Sirunyan et al., Search for new physics in events with two soft oppositely charged leptons and missing transverse momentum in proton-proton collisions at $\sqrt{s} = 13$ TeV, Phys. Lett. B 782 (2018) 440 [1801.01846].
- [158] CMS collaboration, A. M. Sirunyan et al., Search for supersymmetry in final states with two oppositely charged same-flavor leptons and missing transverse momentum in proton-proton collisions at $\sqrt{s} = 13$ TeV, JHEP **04** (2021) 123 [2012.08600].
- [159] CMS collaboration, A. M. Sirunyan et al., Combined search for electroweak production of charginos and neutralinos in proton-proton collisions at $\sqrt{s} = 13$ TeV, JHEP **03** (2018) 160 [1801.03957].
- [160] ATLAS collaboration, M. Aaboud et al., Search for electroweak production of supersymmetric particles in final states with two or three leptons at $\sqrt{s} = 13$ TeV with the ATLAS detector, Eur. Phys. J. C 78 (2018) 995 [1803.02762].

- [161] ATLAS collaboration, M. Aaboud et al., Search for chargino-neutralino production using recursive jigsaw reconstruction in final states with two or three charged leptons in proton-proton collisions at $\sqrt{s} = 13$ TeV with the ATLAS detector, Phys. Rev. D 98 (2018) 092012 [1806.02293].
- [162] ATLAS collaboration, G. Aad et al., Search for direct production of electroweakinos in final states with one lepton, missing transverse momentum and a Higgs boson decaying into two b-jets in pp collisions at $\sqrt{s} = 13$ TeV with the ATLAS detector, Eur. Phys. J. C 80 (2020) 691 [1909.09226].
- [163] ATLAS collaboration, M. Aaboud et al., Search for chargino and neutralino production in final states with a Higgs boson and missing transverse momentum at $\sqrt{s} = 13$ TeV with the ATLAS detector, Phys. Rev. D 100 (2019) 012006 [1812.09432].
- [164] CMS collaboration, A. M. Sirunyan et al., Search for new phenomena in final states with two opposite-charge, same-flavor leptons, jets, and missing transverse momentum in pp collisions at $\sqrt{s} = 13$ TeV, JHEP 03 (2018) 076 [1709.08908].
- [165] CMS collaboration, A. M. Sirunyan et al., Search for supersymmetry with Higgs boson to diphoton decays using the razor variables at $\sqrt{s} = 13$ TeV, Phys. Lett. B 779 (2018) 166 [1709.00384].
- [166] ATLAS collaboration, G. Aad et al., Search for electroweak production of charginos and sleptons decaying into final states with two leptons and missing transverse momentum in $\sqrt{s} = 13$ TeV pp collisions using the ATLAS detector, Eur. Phys. J. C 80 (2020) 123 [1908.08215].
- [167] CMS collaboration, A. M. Sirunyan et al., Searches for pair production of charginos and top squarks in final states with two oppositely charged leptons in proton-proton collisions at $\sqrt{s} = 13 \text{ TeV}$, JHEP 11 (2018) 079 [1807.07799].
- [168] ATLAS collaboration, G. Aad et al., Search for charginos and neutralinos in final states with two boosted hadronically decaying bosons and missing transverse momentum in pp collisions at $\sqrt{s} = 13$ TeV with the ATLAS detector, Phys. Rev. D 104 (2021) 112010 [2108.07586].
- [169] ATLAS collaboration, M. Aaboud et al., Search for photonic signatures of gauge-mediated supersymmetry in 13 TeV pp collisions with the ATLAS detector, Phys. Rev. D 97 (2018) 092006 [1802.03158].
- [170] ATLAS collaboration, G. Aad et al., Search for supersymmetry in events with four or more charged leptons in $139fb^{-1}$ of $\sqrt{s} = 13$ TeV pp collisions with the ATLAS detector, JHEP **07** (2021) 167 [2103.11684].
- [171] ATLAS collaboration, G. Aad et al., Searches for electroweak production of supersymmetric particles with compressed mass spectra in $\sqrt{s} = 13$ TeV pp collisions with the ATLAS detector, Phys. Rev. D 101 (2020) 052005 [1911.12606].
- [172] ATLAS collaboration, M. Aaboud et al., Search for electroweak production of supersymmetric states in scenarios with compressed mass spectra at $\sqrt{s} = 13$ TeV with the ATLAS detector, Phys. Rev. D 97 (2018) 052010 [1712.08119].